



The bottom-quark mass from non-relativistic sum rules at NNNLO

M. Beneke^a, A. Maier^a, J. Piclum^{a,b,c}, T. Rauh^a

^a Physik Department T31, James-Frank-Straße 1, Technische Universität München, D-85748 Garching, Germany

^b Institut für Theoretische Teilchenphysik und Kosmologie, RWTH Aachen University, D-52056 Aachen, Germany

^c Albert Einstein Center for Fundamental Physics, Institute for Theoretical Physics, Sidlerstrasse 5, CH-3012 Bern, Switzerland

Received 26 November 2014; accepted 1 December 2014

Available online 4 December 2014

Editor: Tommy Ohlsson

Abstract

We determine the mass of the bottom quark from high moments of the $b\bar{b}$ production cross section in e^+e^- annihilation, which are dominated by the threshold region. On the theory side next-to-next-to-next-to-leading order (NNNLO) calculations both for the resonances and the continuum cross section are used for the first time. We find $m_b^{\text{PS}}(2 \text{ GeV}) = 4.532_{-0.039}^{+0.013} \text{ GeV}$ for the potential-subtracted mass and $m_b^{\overline{\text{MS}}}(m_b^{\overline{\text{MS}}}) = 4.193_{-0.035}^{+0.022} \text{ GeV}$ for the $\overline{\text{MS}}$ bottom-quark mass.

© 2014 The Authors. Published by Elsevier B.V. This is an open access article under the CC BY license (<http://creativecommons.org/licenses/by/3.0/>). Funded by SCOAP³.

1. Introduction

The bottom-quark mass is one of only a handful of fundamental QCD parameters, and thus its precise knowledge is of considerable interest by itself. Furthermore, there are also phenomenological applications which benefit from a small uncertainty in the value of the bottom-quark mass. Examples include Higgs decays to bottom quarks and decays of B mesons.

Sum rules provide a well-established method for the determination of heavy-quark masses [1,2]. Considering the normalised bottom production cross section

E-mail address: a.maier@tum.de (A. Maier).

$$R_b(s) = \frac{\sigma(e^+e^- \rightarrow b\bar{b} + X)}{\sigma(e^+e^- \rightarrow \mu^+\mu^-)}, \quad (1.1)$$

where s is the square of the e^+e^- center-of-mass energy, we can define its moments \mathcal{M}_n as

$$\mathcal{M}_n = \int_0^\infty ds \frac{R_b(s)}{s^{n+1}} = -6\pi i \oint_C ds \frac{\Pi_b(s)}{s^{n+1}} = \frac{12\pi^2}{n!} \left(\frac{d}{dq^2} \right)^n \Pi_b(q^2) \Big|_{q^2=0}. \quad (1.2)$$

Π_b denotes the contribution from bottom quarks to the vacuum polarisation function. C is an arbitrary closed contour that encloses the origin and does not cross the branch cut, i.e. the part of the positive real half-axis where $R_b(s) = 12\pi \text{Im} \Pi_b(s + i\epsilon) > 0$. Quark–hadron duality now permits to determine the bottom-quark mass by equating moments obtained from the measured hadronic cross section with moments calculated from derivatives of the theoretically predicted polarisation function, which can themselves be obtained from the theoretically predicted partonic cross section by the above dispersion relation (1.2).

For small values of n it is most convenient to calculate moments directly from the derivatives of the polarisation function in conventional perturbation theory. As n increases the theory uncertainty grows and for $n \gtrsim 10$ the perturbation series shows no signs of convergence anymore (cf. [3,4]).

For larger values of n the integral over R_b in Eq. (1.2) is increasingly dominated by small kinetic energies $E = \sqrt{s} - 2m_b \sim m_b/n$ [5,6], where m_b is the bottom-quark mass. Thus, the quarks are non-relativistic with a small velocity $v \sim 1/\sqrt{n} \ll 1$. At the same time the strong coupling constant α_s is of the same order as the quark velocity. For this reason terms scaling with powers of α_s/v , which originate from Coulomb interaction, have to be summed to all orders. This is achieved in the effective theory of potential non-relativistic QCD (PNRQCD) [7]. In summary, for large- n , “non-relativistic” moments the power counting for the cross section up to NNNLO is given by

$$R_b \sim v \sum_k \left(\frac{\alpha_s}{v} \right)^k \times \begin{cases} 1 & \text{LO,} \\ \alpha_s, v & \text{NLO,} \\ \alpha_s^2, \alpha_s v, v^2 & \text{NNLO,} \\ \alpha_s^3, \alpha_s^2 v, \alpha_s v^2, v^3 & \text{NNNLO.} \end{cases} \quad (1.3)$$

The admissible values of n are limited by the requirement that the ultrasoft scale m_b/n remains larger than the intrinsic strong interaction scale of a few hundred MeV [8].

In this work we present the first determination of the bottom-quark mass from large- n sum rules at next-to-next-to-next-to-leading order (NNNLO). The corresponding NNLO calculations have been done about fifteen years ago [8–10]. A partial NNNLO result that uses NNNLO accuracy for the bound-state contribution and NNLO accuracy for the continuum contribution to the moments appeared recently [11]. The outline of this paper is as follows. First, in Section 2, we derive the values of the relevant moments from experimental data. We proceed in Section 3 with an outline of the corresponding PNRQCD calculation and a discussion of suitable mass schemes. In Section 4 we summarise our results for R_b and for the bottom-quark mass and compare them to other recent high-precision sum rule analyses. For the comparison we consider the works by Chetyrkin et al. [12], Hoang et al. [13], and Penin and Zerf [11]. We conclude in Section 5. Since we are aiming at high precision, we include the effects of the non-zero charm-quark mass. The details of this computation are given in four appendices.

Table 1

Contributions to the experimental moments $\mathcal{M}_n^{\text{exp}}$ in $(10 \text{ GeV})^{-2n}$.

n	6	7	8	9	10
Resonances	0.1861(20)	0.2004(22)	0.2166(24)	0.2351(27)	0.2560(29)
Continuum	0.0240(85)	0.0182(58)	0.0140(41)	0.0110(29)	0.0088(21)
Total	0.2101(88)	0.2185(62)	0.2307(47)	0.2461(39)	0.2648(36)
n	11	12	13	14	15
Resonances	0.2797(33)	0.3064(36)	0.3364(40)	0.3702(45)	0.4081(50)
Continuum	0.0070(15)	0.0057(11)	0.0046(8)	0.0038(6)	0.0031(4)
Total	0.2867(36)	0.3120(38)	0.3410(41)	0.3740(45)	0.4112(50)

2. Experimental moments

For sufficiently large values of n the experimental moments $\mathcal{M}_n^{\text{exp}}$ are dominated by Υ bound states. In the narrow-width approximation for the resonances $\Upsilon(1S)$ to $\Upsilon(4S)$ we obtain

$$\mathcal{M}_n^{\text{exp}} = 9\pi \sum_{N=1}^4 \frac{1}{\alpha(M_{\Upsilon(NS)})^2} \frac{\Gamma_{\Upsilon(NS) \rightarrow l^+l^-}}{M_{\Upsilon(NS)}^{2n+1}} + \int_{s_{\text{cont}}}^{\infty} ds \frac{R_b(s)}{s^{n+1}}, \quad (2.1)$$

where we take the current PDG values [14] for the masses $M_{\Upsilon(NS)}$ and the leptonic widths $\Gamma_{\Upsilon(NS) \rightarrow l^+l^-}$ of the Υ resonances. In the energy region of interest we approximate the running QED coupling by a constant value, which is given in terms of the fine structure constant by $\alpha(2m_b) \approx 1.036\alpha$ [15].

For the remaining continuum integral we use experimental data [16] corrected for initial state radiation between $\sqrt{s_{\text{cont}}} = 10.6178 \text{ GeV}$ and 11.2062 GeV (see [12] for details). In the absence of data for higher center-of-mass energies we assume R_b to stay roughly constant with $R_b = 0.3 \pm 0.2$. For $n = 6, 10, 15$ the unknown high-energy part constitutes approximately 53%, 35%, 21% of the total continuum contribution, respectively. The large uncertainty of this part is therefore not expected to be important. The resulting values and uncertainties for the experimental moments are shown in Table 1.

3. Theory moments

3.1. The cross section in PNRQCD

The normalised cross section for bottom production at NNNLO in PNRQCD has the form

$$R_b = 12\pi e_b^2 \text{Im} \left[\frac{N_c}{2m_b^2} \left(c_v \left[c_v - \frac{E}{m_b} \left(c_v + \frac{d_v}{3} \right) \right] G(E) + \dots \right) \right], \quad (3.1)$$

see e.g. [17]. e_b and m_b are the bottom quark's fractional electric charge and pole mass, respectively. E is the kinetic energy with the usual relation $E = \sqrt{s} - 2m_b$ to the center-of-mass energy \sqrt{s} . c_v and d_v are the matching coefficients of the non-relativistic vector current, i.e.

$$j^i = c_v \psi^\dagger \sigma^i \chi + \frac{d_v}{6m_b^2} \psi^\dagger \sigma^i \mathbf{D}^2 \chi + \dots, \quad (3.2)$$

where j^i are the spatial components of the relativistic current $\bar{b}\gamma^\mu b$, and ψ (χ) the non-relativistic quark (antiquark) spinors. Finally, $G(E)$ is the non-relativistic current correlator

$$G(E) = \frac{i}{2N_c(d-1)} \int d^d x e^{iEx^0} \langle 0 | T [\chi^\dagger \sigma^i \psi](x) [\psi^\dagger \sigma^i \chi](0) | 0 \rangle \Big|_{\text{PNRQCD}} \quad (3.3)$$

in d space–time dimensions.

Below threshold, i.e. for $E < 0$, $G(E)$ develops infinitely many poles which can be interpreted as S -wave, spin-1 $b\bar{b}$ bound states. In the vicinity of such a bound state $G(E)$ behaves as

$$G(E) \xrightarrow{E \rightarrow E_N} \frac{|\psi_N(0)|^2}{E_N - E - i\epsilon}, \quad (3.4)$$

where $\psi_N(0)$ is the bound state wave function at the origin while E_N is the binding energy. Splitting off the bound-state contribution we can thus write the moments as

$$\mathcal{M}_n^{\text{th}} = \frac{12\pi^2 N_c e_b^2}{m_b^2} \sum_{N=1}^{\infty} \frac{Z_N}{(2m_b + E_N)^{2n+1}} + \int_{4m_b^2}^{\infty} ds \frac{R_b(s)}{s^{n+1}} \quad (3.5)$$

with the residues

$$Z_N = c_v \left[c_v - \frac{E_N}{m_b} \left(c_v + \frac{d_v}{3} \right) \right] |\psi_N(0)|^2 + \dots \quad (3.6)$$

Note that Z_N is a physical quantity, while the wave function $\psi_N(0)$ and the matching coefficients separately depend on the factorisation scale and scheme that separates short- and long-distances.

R_b (3.1) and Z_N (3.6) are understood to be strictly expanded up to NNNLO according to the PNRQCD power counting (1.3). For example, terms of order α_s^4 and higher that are generated through the product of lower-order terms are to be dropped. Contrarily, we will leave the factor $(2m_b + E_N)^{-(2n+1)}$ in Eq. (3.5) unexpanded for reasons discussed in Section 3.3. Not expanding this factor is equivalent to resumming the poles back into the polarisation function (cf. [18]), i.e. replacing

$$\Pi_b \rightarrow \Pi_b + \frac{3e_b^2}{2m_b^2} \sum_{N=1}^{\infty} \left\{ \frac{[Z_N]_{\text{expanded}}}{[E_N - E]_{\text{unexpanded}}} - \left[\frac{Z_N}{E_N - E} \right]_{\text{expanded}} \right\} \quad (3.7)$$

in the contour integral that defines the moments (1.2).

3.2. Technical implementation

We require the following ingredients for the NNNLO analysis of non-relativistic moments:

- The hard Wilson coefficient c_v at order α_s^3 [19] and d_v at order α_s [20].
- The third-order corrections to the S -wave energy levels E_N [21–23], to the wave functions ψ_N at the origin [22–24] and to $G(E)$ [23,25] from non-relativistic potentials up to NNNLO [17,26–30].
- Ultrasoft corrections to these quantities [31–33].

For an extensive overview of all third-order corrections see [17,25].

Note that the results in [25,33] are calculated for the case of top quarks, that is in the complex energy plane for finite imaginary part Γ corresponding to the top-quark width. The application of these results to bottom quarks requires to take the limit $\Gamma \rightarrow 0$, which is non-trivial, since the analytic expressions cannot be straightforwardly evaluated numerically for vanishing width. In [33]

the $\Gamma = 0$ result has been constructed for the ultrasoft contribution by extrapolation. Evaluating the third-order potential corrections given in [25] for real energy E requires a substantial amount of extra work, which we briefly discuss in the following.

The higher-order potential corrections to the Green function are expressed in terms of nested harmonic sums, sums over gamma and polygamma functions, and generalised hypergeometric functions [23,25]. The complex variable $\lambda = (\alpha_s C_F/2)\sqrt{-m/(E+i\Gamma)}$ appears for example in the argument of (poly-)gamma functions or as one of the parameters of the hypergeometric functions. In our application, we have to evaluate the Green function for positive values of the energy E , starting at $E = 0$. For vanishing width Γ , λ tends to $+i\infty$ as E tends to zero. Thus, we have to ensure that all expressions are well-defined in this limit and that their numerical evaluation is possible.

In most cases it is possible to express the correction to the Green function in terms of harmonic sums. This is in particular the case for most of the generalised hypergeometric functions, which can be treated as described in Appendix A.1 of [34]. The harmonic sums can then be analytically continued with the methods of [35,36]. However, in some cases the correction to the Green function is expressed in terms of single or even double sums which could not be expressed as nested harmonic sums. For such sums it was often necessary to truncate the summation at some (λ -dependent) value and construct suitable asymptotic expansions to approximate the remainder. In all cases we have checked that the numerical precision is sufficient for our extraction of the bottom-quark mass, such that the numerical uncertainty can be neglected.

A relatively simple example of this procedure is given by the sum

$$\sum_{k=1}^{\infty} \frac{[(k-\lambda)(\psi(k-\lambda) - \psi(k)) + k\lambda\psi^{(1)}(k)]^2}{k}, \quad (3.8)$$

which appears in the insertion of the Darwin term. Here ψ is the logarithmic derivative of the gamma function and $\psi^{(1)}$ the first derivative of ψ . The sum converges only slowly when λ is large, which makes the numerical evaluation difficult. Therefore, we introduce a cut-off Λ for the summation and explicitly sum all terms up to this cut-off. Choosing Λ to be much larger than $|\lambda|$, we can approximate the remainder by expanding the summand in the limit $k \rightarrow \infty$. Note that for $\psi(k-\lambda)$ this is not simply an expansion in $|\lambda|/k$, but rather a double expansion for $k \gg 1$ and $k \gg |\lambda|$. In the first step the entire argument of the ψ function is considered large and the terms of the resulting asymptotic series are further expanded for $|\lambda|/k \rightarrow 0$ in the second step, yielding

$$\begin{aligned} \psi(k-\lambda) &= \ln(k-\lambda) - \frac{1}{2(k-\lambda)} - \frac{1}{12(k-\lambda)^2} + \frac{1}{120(k-\lambda)^4} + \mathcal{O}\left(\frac{1}{(k-\lambda)^6}\right) \\ &= \ln k - (1+2\lambda)\frac{1}{2k} - (1+6\lambda+6\lambda^2)\frac{1}{12k^2} - (\lambda+3\lambda^2+2\lambda^3)\frac{1}{6k^3} \\ &\quad + (1-30\lambda^2-60\lambda^3-30\lambda^4)\frac{1}{120k^4} + \mathcal{O}\left(\frac{1}{k^5}\right). \end{aligned} \quad (3.9)$$

After expanding the summand in (3.8), the sum over k from $\Lambda+1$ to infinity can be evaluated in terms of Hurwitz zeta functions (in more complicated cases we also encounter derivatives of this function). The first three terms are

$$\frac{\lambda^4}{4}\zeta(3, \Lambda+1) + \frac{\lambda^5}{6}\zeta(4, \Lambda+1) + \frac{\lambda^4}{36}(-3+4\lambda^2)\zeta(5, \Lambda+1), \quad (3.10)$$

where $\zeta(s, a) = \sum_{k=0}^{\infty} (k+a)^{-s}$. Due to the nature of the double expansion of $\psi(k-\lambda)$, higher order terms in this series can have the same powers of λ as lower order ones. However, these terms are still suppressed by additional powers of Λ , since the first argument of ζ increases with each term and $\zeta(s, \Lambda)$ with $s > 1$ behaves like $1/\Lambda^{s-1}$ as Λ tends to infinity. In practice, we fix for each sum an appropriate expansion depth N_{\max} for the remainder. This makes it possible to speed-up the calculation by pre-computing the expansion for arbitrary values of the cut-off. The latter is then determined at runtime as $\Lambda = \max(\Lambda_0, f|\lambda|)$, where Λ_0 is a lower limit for the cut-off and f is a positive integer. Λ_0 and f are again chosen separately for each sum. In the above example we use $N_{\max} = 15$, $\Lambda_0 = 100$, and $f = 2$. By varying N_{\max} and f , we can check the numerical stability of the procedure.

3.3. Mass schemes

It is well known that for quark masses the pole scheme is ambiguous due to its sensitivity to infrared renormalons [37–39]. Numerous short-distance mass schemes have been developed to cure this shortcoming [40–43]. In this work we consider the potential-subtracted (PS) mass introduced in [41] and the mass in the $\overline{\text{MS}}$ scheme. They are related to the pole mass via perturbative series of the form

$$m_b = m_b^M + \sum_{i=0}^{\infty} \delta m_i^M, \quad M = \text{PS}, \overline{\text{MS}}. \quad (3.11)$$

For the cancellation of leading infrared renormalons we have to take into account the first correction term δm_0^M already at leading order and one additional correction term for each further order in the PNRQCD expansion.

In the PS scheme the leading subtraction term is given by

$$\delta m_0^{\text{PS}} = \frac{\alpha_s(\mu) C_F}{\pi} \mu_f, \quad (3.12)$$

where we choose the subtraction scale as $\mu_f = 2 \text{ GeV}$. The choice of the renormalisation scale μ is discussed in Section 4.1. The higher-order terms up to δm_3^{PS} required for our NNNLO analysis can be found in [23].

In the $\overline{\text{MS}}$ scheme the higher-order corrections in relation (3.11) are only known up to $i = 2$ [44,45].¹ It is, however, expected that the correction terms $\delta m_i^{\overline{\text{MS}}}$ are dominated by the leading infrared renormalon already at relatively low orders [46,47]. On this basis an approximation was constructed in [43,48]. The deviation from the known result is about 10% for $i = 1$ and less than 1% for $i = 2$. We employ this approximation for $i = 3$, which corresponds to setting the correction term $\delta m_3^{\overline{\text{MS}}}$ at the scale $m_b^{\overline{\text{MS}}}$ to $\tilde{r}_3 m_b^{\overline{\text{MS}}} \alpha_s^4 \approx 13.59(83) m_b^{\overline{\text{MS}}} \alpha_s^4$ in the notation of [43]. The error range encompasses the value $\tilde{r}_3 = 13.5972$ obtained from the large- β_0 approximation [46,47].

When eliminating the pole mass in the cross section formulae in favour of a short-distance mass the question arises whether the resulting expression should be expanded in the correction terms δm_i^M , $i \geq 1$. For the $\overline{\text{MS}}$ scheme such an expansion is not sensible in the threshold region [41]. This can for instance be seen by considering the factor $(2m_b + E_N)^{-(2n+1)}$ in the resonance contribution to the theory moments (3.5). On the one hand, the correction of order i

¹ Note that in our notation $\delta m_i^{\overline{\text{MS}}}$ denotes the $(i+1)$ -loop correction.

to the energy levels E_N is parametrically of the same order as $\delta m_{i+1}^{\overline{\text{MS}}}$ according to the PNRQCD power counting $\alpha_s \sim v \ll 1$. On the other hand, renormalon cancellation only occurs between the correction of order i to the binding energies and $\delta m_i^{\overline{\text{MS}}}$, so an expansion consistent with our power counting would spoil this cancellation.

In the PS scheme both expanding and not expanding the PS–pole mass relation (3.11) appear to be viable options. However, as discussed in [25], an expansion induces unphysical behaviour near threshold in the continuum cross section. Therefore we will not expand the cross section in δm_i^{PS} , which corresponds to the PS-shift (PSS) prescription of [25]. At the same time this again implies that the entire factor $(2m_b + E_N)^{-(2n+1)}$ must remain unexpanded to ensure the cancellation of leading infrared renormalons. In practice, this means that in both schemes, for given m_b^M and order N^kLO, we first compute m_b from (3.11) truncating the sum at $i = k$ and add the bound state energy evaluated to the same order.

3.4. Expansion in the kinetic energy

Up to now, in (3.1), (3.5) and (3.6) an overall factor of $1/s$ stemming from the relativistic polarisation function has been expanded for $E \ll m_b$. Since we chose not to expand the factor $1/s^{n+1}$ in the definition (1.2) of the moments, we may also contemplate to keep this factor unexpanded. The corresponding expressions, denoted by a tilde, take the following forms:

$$\tilde{R}_b = 12\pi e_b^2 \text{Im} \left[\frac{2N_c}{s} \left(c_v \left[c_v - \frac{E}{m_b} \frac{d_v}{3} \right] G(E) + \dots \right) \right], \quad (3.13)$$

$$\tilde{Z}_N = c_v \left[c_v - \frac{E_N}{m_b} \frac{d_v}{3} \right] |\psi_N(0)|^2 + \dots, \quad (3.14)$$

$$\tilde{\mathcal{M}}_n^{\text{th}} = 48\pi^2 N_c e_b^2 \sum_{N=1}^{\infty} \frac{\tilde{Z}_N}{(2m_b + E_N)^{2n+3}} + \int_{4m_b^2}^{\infty} ds \frac{\tilde{R}_b(s)}{s^{n+1}}. \quad (3.15)$$

Formally, the difference to (3.1), (3.5) and (3.6) is of higher order (NNNNLO).

These higher-order corrections are numerically non-negligible, possibly due to sub-leading renormalon contributions. For the N th resonance $1/s$ assumes the form $(2m_b + E_N)^{-2}$, where renormalon contributions cancel between the binding energy and the mass. If we now expand this factor for $E_N \ll m_b$ and, according to the PNRQCD power counting, discard contributions to E_N that are beyond NLO the renormalon cancellation will again be spoiled. Since the exponent now is not of order n as was the case for the $1/s^{n+1}$ factor, the generated renormalon ambiguity is only of order Λ_{QCD}/m_b and therefore sub-leading. Since this is not the only source of sub-leading renormalon contributions, in order to decide which prescription for the expansion of $1/s$ is the preferred one it would be necessary to analyse carefully how all of these contributions can be cancelled in the determination of the moments. To our knowledge such an analysis has not been performed yet. We will find in Section 4.3 that not expanding the factor $1/s$ in the polarisation function improves the consistency of mass values extracted from different moments. In the following, we will therefore mainly concentrate on the “unexpanded” moments defined by (3.15). We then check that the difference to the “expanded” approach is compatible with our estimate of the perturbative uncertainty.

3.5. Charm-quark mass effects

The ingredients for the NNNLO cross section described in Section 3.1 all assume the light quarks to be massless, which is well justified as long as the light-quark masses are smaller than the physical scales that appear in the problem. However the actual charm-quark mass is of the order of the soft scale (inverse Bohr radius) $m_b\alpha_s \sim m_b v$ of the $b\bar{b}$ system near threshold and therefore has to be included in a consistent treatment. At NNLO the effects of a non-zero charm-quark mass on the moments have been discussed thoroughly in [49], where they were found to lead to a sizeable shift of around -30 MeV in the extracted $\overline{\text{MS}}$ bottom-quark mass.

Since the factor $1/s^{n+1}$ in the moments is expanded non-relativistically in [49] the results cannot be included in our expressions (3.5) and (3.15). In the following we discuss in which steps in the computation of the cross section the effects of a non-zero charm-quark mass are relevant and determine the missing contributions up to NNLO. The NNNLO charm-mass effects are unknown at the time of this writing and their determination is clearly outside the scope of this work.

The computation of the cross section proceeds in three separate steps, which are the hard matching, the soft matching and the computation of the spectral function in the resulting effective theory PNRQCD, as was discussed in detail in [17]. Since m_c is considered to be soft the results of the hard matching must be analytic in $m_c^2/m_b^2 \sim \alpha_s^2$ and charm-mass effects due to the insertion of a charm loop into a gluon line scale as $\alpha_s^2 m_c^2/m_b^2 \sim \alpha_s^4$ compared to α_s for the gluon line without charm-loop insertion. To NNNLO the hard matching procedure is therefore unaffected.

In the soft matching procedure the charm quark is integrated out. The only part of the resulting PNRQCD Lagrangian that is affected at NNLO is the Coulomb potential, which can be split in two parts

$$V = V_{\text{massless}} + V_{m_c}, \quad (3.16)$$

where V_{m_c} is defined such that it vanishes for $m_c \rightarrow 0$.² It has been computed to two loops in [50, 51]; convenient representations are given in [49]. In order to offer a self-contained discussion we quote these results in Appendix A. As discussed in [17] the soft matching of the external vector current with massless light quarks is trivial to all orders, because the respective integrals are scaleless. The introduction of the charm-quark mass as a soft scale means that starting at two loops this is no longer true. However the corresponding matching coefficient must be trivial in the limit $m_c \rightarrow 0$ and since the only other scale relevant for the external current is m_b , the correction must contain at least one power of m_c/m_b , which again is beyond NNLO.³

The spectral function receives contributions from the charm-quark mass through insertions of the Coulomb potential. At NLO only the single insertion of $V_{m_c}^{(1)}$ is required. At NNLO the single insertion of $V_{m_c}^{(2)}$ and the double insertions of $V_{m_c}^{(1)}$ and $V_{\text{massless}}^{(1)}$ as well as twice $V_{m_c}^{(1)}$ contribute. Our results for the charm corrections to the energy levels E_N and the wave functions $|\psi_N(0)|^2$ can be found in Appendix C. We find numerical agreement in those parts that are available in the literature [49,52].

² The effects of integrating out the charm quark on the running of α_s can be included in the Coulomb potential. We follow the convention of [49], where the potential is defined for α_s evolving with $n_{l,\text{massless}} + 1$ flavors.

³ We have also checked explicitly that the term without any power of m_c/m_b cancels upon wave function renormalisation.

Table 2

Contributions of a non-zero charm-quark mass to the binding energy $E_{1,m_c}^{(i)} = E_1^{(0)} e_{1,m_c}^{(i)}$ and wave function of the $\Upsilon(1S)$ resonance. The corrections to the wave function are given by $|\psi_1(0)|^2 = |\psi_1^{(0)}(0)|^2 (1 + \sum_{i=1}^{\infty} f_1^{(i)})$, and $f_{1,m_c}^{(i)}$ denotes the charm correction to $f_1^{(i)}$. The results are given in the pole-mass scheme with the input values $m_b = 5$ GeV, $\mu = 5$ GeV, $\alpha_s(5 \text{ GeV}) = 0.2135$ and $m_c(5 \text{ GeV}) = 0.892$ GeV. To demonstrate the large cancellation in the $\Upsilon(1S)$ mass $M_{\Upsilon(1S)} = 2m_b + E_1 = 2m_b^{\text{PS}} + 2\sum_{i=1}^{\infty} \delta m_i^{\text{PS}} + E_1$ once a short-distance mass scheme is used, we also show results for the charm-mass effects in the relation between the PS and pole mass with $\mu_f = 2$ GeV. $2\delta m_{i,m_c}^{\text{PS}}$ and $E_{1,m_c}^{(i)}$ are given in MeV, while $f_{1,m_c}^{(i)}$ is dimensionless.

$N = 1$	$2\delta m_{1,m_c}^{\text{PS}}$	$2\delta m_{2,m_c}^{\text{PS}}$	$E_{1,m_c}^{(1)}$	$E_{1,m_c}^{(2)}$	$f_{1,m_c}^{(1)}$	$f_{1,m_c}^{(2)}$
single insertion $\{m_c\}$	9.50	23.21	−6.82	−18.02	0.0335	0.0644
double insertions						
$\{m_c, \text{massless}\}$	−	−	−	−1.46	−	−0.0043
$\{m_c, m_c\}$	−	−	−	−0.02	−	−0.0001
Σ	9.50	23.21	−6.82	−19.50	0.0335	0.0600

Since, for the reasons discussed in Section 3.3, we use the PS or $\overline{\text{MS}}$ mass instead of the pole mass in the cross section as well as the moments, the charm-mass effects also have to be considered in the relation between different mass schemes. In the conversion between the pole and the $\overline{\text{MS}}$ scheme, these effects are known at order α_s^3 [53]. For our analysis we have also computed the corresponding corrections to the relation between the PS and the pole mass. These results are summarised in Appendix B.

Anticipating our numerical analysis in Section 4 let us now discuss the impact of a non-zero charm-quark mass. We parametrise the corrections in terms of the $\overline{\text{MS}}$ charm-quark mass at our overall renormalisation scale μ , which we obtain via 4-loop running from the initial value $m_c^{\overline{\text{MS}}}(3 \text{ GeV}) = 0.986$ GeV [12].⁴ It should be noted that effects from a non-zero charm-quark mass are expected to be large for quantities that have large infrared sensitivity. The reason for this is that the charm-loop correction effectively acts as an infrared cut-off on the virtuality of the gluon line into which it is inserted.

Table 2 illustrates the numerical impact of a non-zero charm-quark mass on the first energy level and the corresponding wave function at the origin and demonstrates the cancellations in the transition to a short-distance mass scheme. Let us now discuss the effect on the final value of the $\overline{\text{MS}}$ bottom-quark mass extracted from the tenth moment. If, at first, we only consider the corrections from single insertions to the binding energies and the wave functions at NNLO (NLO) the resulting mass value receives a shift of +16 MeV (+4 MeV). In line with our previous discussion we expect a considerable compensation from the charm effects in the relation between the infrared-sensitive pole mass and the PS mass. In fact, including also these corrections the mass shift reduces to around +0.5 MeV (−0.5 MeV). The cancellation of infrared contributions can also be observed analytically. Expanding all corrections in the limit of a small charm-quark mass, the linear terms in the expansion cancel exactly between the corrections to the energy levels and wave functions on the one side and the relation between PS and pole mass on the other side (cf. [49]). The charm mass corrections to the relation between the PS and the $\overline{\text{MS}}$ scheme are relatively small; adding them to the analysis leads to a total shift of −3.5 MeV (−2 MeV) in the $\overline{\text{MS}}$ bottom-quark mass.

⁴ To compute the renormalisation group evolution we employ either RunDec [54] or a custom implementation.

Up to now, we have neglected charm corrections to double insertions and to the continuum cross section. In agreement with [49] we find that the charm contributions from double insertions are suppressed compared to the single insertions, causing an additional mass shift of only +0.5 MeV. Since the overall continuum contribution to the tenth moment is already small we expect charm effects in the cross section above threshold to be negligible. Indeed we find an extra shift of less than 0.1 MeV from the NLO corrections listed in Appendix D. In the light of these findings we will use the computationally expensive charm corrections to the continuum cross section and the double insertions only to extract our central value and neglect them in the error analysis.

To account for the unknown NNNLO charm-mass corrections we assign an uncertainty given by the difference between the bottom-quark mass obtained at NNLO for the physical value of the charm-quark mass and the bottom-quark mass obtained in the limit of a vanishing charm-quark mass.

Concerning the size of the charm corrections there is a large discrepancy between the final mass shift of -3 MeV in our analysis and about -30 MeV in [49]. We find that differences between the two approaches, such as the choice of renormalisation scales, expansion of factors $1/s$, and different values for the charm-quark mass, cannot account for this disparity. It seems suspicious that [49] claims large effects of around 50% for $n = 20$. Such high moments are dominated by the first resonance. By the definition of the $1S$ mass, however, charm effects cancel completely in the combination $2m_b^{1S} + 2\sum_{i=1}^{\infty}\delta m_i^{1S} + E_1 \equiv 2m_b^{1S}$. Thus, only the charm corrections to the residue Z_1 contribute. These effects are independent of n , and, according to our findings, rather moderate in size (cf. Table 2).

4. Numerical analysis

4.1. Choice of the renormalisation scale

Since the moments receive contributions from several distinct physical regions it is important to choose an adequate value for the overall renormalisation scale μ . A priori “natural” options include the hard scale $\mu \sim m_b$, the soft scale $\mu \sim 2m_b/\sqrt{n}$ and the ultrasoft scale $\mu \sim m_b/n$. In this work we do not consider the possibility of summing logarithmic effects $\ln\sqrt{n}$ related to the presence of different scales by renormalisation group methods (see [13] in the present context), since $\ln\sqrt{10}$ is not a particularly large number. Fig. 1 shows the scale dependence of the tenth moment for μ between 2 GeV and 10 GeV at different orders. There is clearly no convergence of the perturbation series for $\mu \lesssim 3$ GeV.⁵ We therefore adopt $\mu = m_b^{\text{PS}}$ as our central scale and vary μ between 3 GeV and 10 GeV to estimate the uncertainty. Note that there is no overlap in the moment values at NLO and NNLO over the entire scale range, which is one of the motivations to perform the third-order calculation. The figure shows that the NNNLO curve lies within the interval determined by the NNLO scale variation.

4.2. Comparison to the fixed-order continuum

The present work is the first to include the continuum cross section with NNNLO accuracy (heavily relying on the input from [25,33] as described in Section 3.2), which is also the most

⁵ A similar observation was made for the leptonic decay width of the $\Upsilon(1S)$ resonance [28].

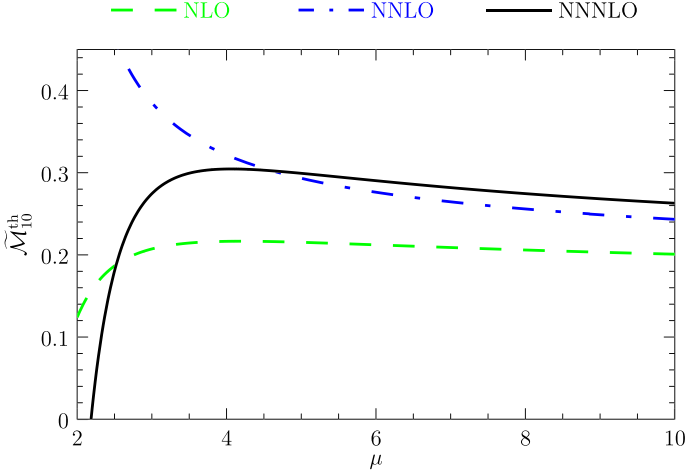


Fig. 1. Scale dependence of the tenth moment $\tilde{\mathcal{M}}_{10}^{\text{th}}$ in $(10 \text{ GeV})^{-20}$ for $\alpha_s(M_Z) = 0.1184$ and $m_b^{\text{PS}}(2 \text{ GeV}) = 4.5 \text{ GeV}$.

complicated part of the NNNLO calculation. Since sum rule determinations of the bottom-quark mass rely on quark–hadron duality, the continuum is conceptually a crucial ingredient in the analysis.

The summation of factors α_s/v implicit in the PNRQCD calculation of the correlator $G(E)$ is only necessary close to threshold. It is therefore reasonable to expect that there is a region with $\alpha_s \ll v \ll 1$ where the continuum cross section can be calculated reliably both in PNRQCD (requiring $v \ll 1$) and conventional perturbation theory (requiring $v \gg \alpha_s$). In Fig. 2 we show the respective predictions adopting the pole-mass scheme with $m_b = 5 \text{ GeV}$, and without expanding the factor $1/s$ in the polarisation function (see Section 3.4). For the fixed-order curves we have used the analytically known result up to order α_s [55] and Padé approximation [56–58] at orders α_s^2 and α_s^3 .

At NLO and NNLO (upper panel) there is apparently a good agreement between the two theories for $v \sim 0.4$. The NNNLO curve in PNRQCD (lower panel), however, lies significantly below the NNLO and the fixed-order curves and shows a very strong dependence on the renormalisation scale.⁶ For smaller scales μ we even observe unphysical negative values for \tilde{R}_b .

One reason for the considerable difference between fixed-order QCD and PNRQCD at NNNLO may be the limited information from the threshold region used for the Padé approximation. In particular, the behaviour of the NNNLO fixed-order curve for $v \rightarrow 0$ is by construction determined by the naive expansion of the NNLO PNRQCD polarisation function to order α_s^3 [57,58]. Although they are suppressed by an additional factor of v , corrections from NNNLO PNRQCD could alter this behaviour considerably as the NNNLO PNRQCD result differs significantly from the NNLO one.

One example for such a big missing correction is given by the product of the third-order correction to the hard Wilson coefficient and the leading-order $G(E)$. Parametrically this correction is of order $v\alpha_s^3$. Due to the numerically large factors involved it still causes a shift of $\Delta R_b \sim -0.2$

⁶ Note that for the $\Upsilon(1S)$ resonance the behaviour of the NNNLO correction under scale variation is much better, see [28].

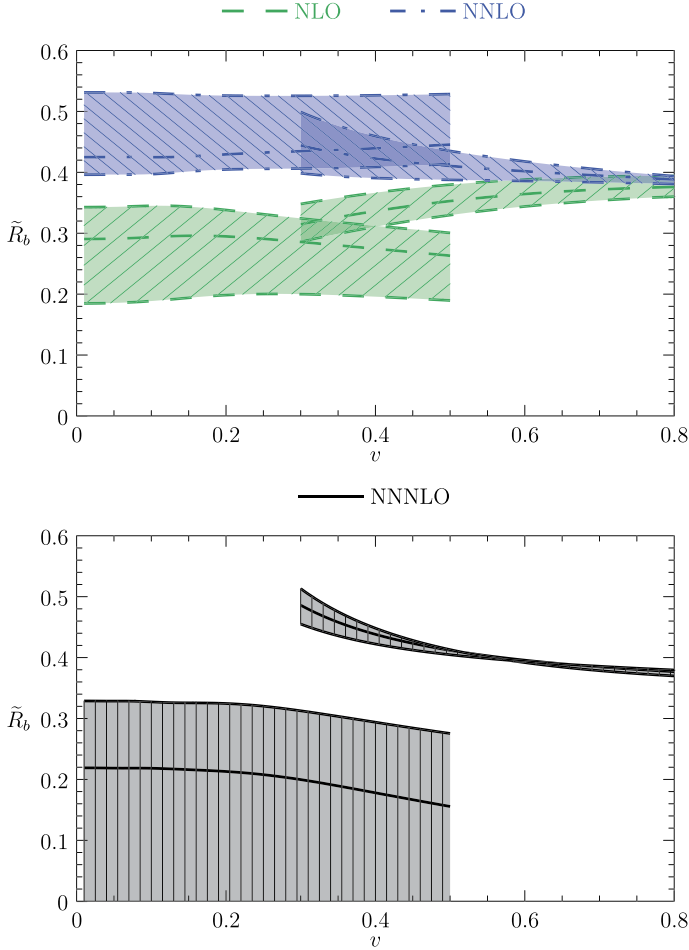


Fig. 2. Behaviour of \tilde{R}_b as a function of $v = \sqrt{E/m_b}$ for a pole mass of $m_b = 5$ GeV. The curves on the left show the PNRQCD prediction, whereas the curves on the right correspond to fixed-order perturbation theory. The shaded areas show the uncertainty from varying the renormalisation scale between 3 GeV and 10 GeV.

at $v = 0.4$. At higher orders in α_s there will be further sizeable contributions from this product, e.g. an additional negative shift of -0.2 at order $\alpha_s^4 v^0$.

While it may be possible to reconcile the discrepancy between the relativistic fixed-order and PNRQCD predictions there still remains the problem that the convergence of the continuum cross section in resummed non-relativistic perturbation theory appears to be quite poor. Neither the difference between consecutive orders nor the scale uncertainty shrink when considering higher-order corrections to the continuum cross section. In fact, at NNNLO the scale uncertainty is much larger than at any lower order.

In our analysis, however, we are of course not interested in the continuum cross section itself but in non-relativistic moments. These are expected to receive their dominant contribution from the resonances. Fig. 3 shows the continuum contribution to the tenth moment at different orders in perturbation theory as a function of the renormalisation scale $3 \text{ GeV} < \mu < 10 \text{ GeV}$. As expected we observe that the continuum contribution at NNNLO is rather small, amounting to less than

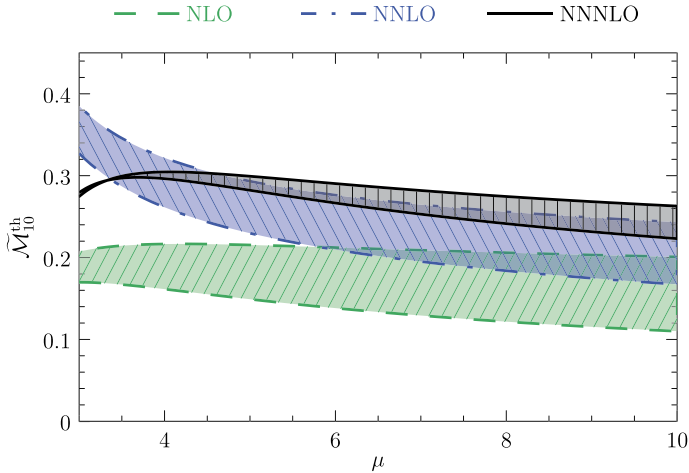


Fig. 3. Scale dependence of $\tilde{\mathcal{M}}_{10}^{\text{th}}$ in $(10 \text{ GeV})^{-20}$ with $m_b^{\text{PS}}(2 \text{ GeV}) = 4.5 \text{ GeV}$. At each order the shaded band shows the contribution from the continuum cross section. The lower boundary of the band is the moment without the continuum contribution.

5% at our central scale $\mu = m_b$ and about 15% at $\mu = 10 \text{ GeV}$. Furthermore, the continuum contribution reduces both the distance between consecutive orders and the scale dependence at each order. We conclude that the seemingly problematic behaviour of the continuum cross section does not impede the extraction of the bottom-quark mass from large- n moments at NNNLO.

4.3. Determination of the bottom-quark mass

We are now in a position to determine the bottom-quark mass by requiring $\mathcal{M}_n^{\text{th}} = \mathcal{M}_n^{\text{exp}}$ for moments with $n \approx 10$. We first eliminate the pole mass in favour of the PS mass $m_b^{\text{PS}}(\mu_f)$, and then convert the resulting mass to the $\overline{\text{MS}}$ scheme. Irrespective of the order of the moments we always perform the conversion at order α_s^4 . As a part of our error analysis we will also first convert to the $\overline{\text{MS}}$ mass $m_b^{\overline{\text{MS}}}(\bar{\mu})$ at an intermediate scale $\bar{\mu}$, which we keep separate from the overall renormalisation scale μ , and then use renormalisation group evolution to find the scale-invariant mass $m_b^{\overline{\text{MS}}}(m_b^{\overline{\text{MS}}})$.

To estimate the error of the resulting mass value for a given moment \mathcal{M}_n we consider the following sources of uncertainties.

- Experimental uncertainty. We add in quadrature the errors induced by uncertainties in the Υ masses, the leptonic widths, the BaBar data directly above the resonances [16], and our estimate $0.1 \leq R_b \leq 0.5$ in the high-energy region.
- Unknown higher-order corrections. As detailed in Section 4.1 we choose the extracted PS mass as our central renormalisation scale and vary μ between 3 GeV and 10 GeV.
- Uncertainty in the strong coupling. We evolve $\alpha_s(m_Z) = 0.1184$ down to our central scale using four-loop running, and decouple the bottom quark at $\mu_{\text{thr}} = 2m_b$. The exact choice of the decoupling scale is numerically irrelevant. When varying the renormalisation scale we remain in the four-flavour theory. To determine the uncertainty in the strong coupling we vary its value at the scale of the Z boson mass by ± 0.0010 .

- QED effects. In our analysis, we include the leading correction in the conversion to the $\overline{\text{MS}}$ mass scheme and the QED Coulomb potential. Assuming $\alpha \sim \alpha_s^2$, these effects are formally of NLO. In practice, we find a shift of less than 1 MeV in the extracted quark mass.
- Number of theoretical resonances. In practice we only take into account the contribution from the first six resonances in the formulae (3.5), (3.15) for the theoretical moments and estimate the resulting uncertainty from the difference to considering only four resonances.
- Scheme conversions. When extracting the PS mass, we vary μ_f between 1 GeV and 3 GeV. In the conversion to the $\overline{\text{MS}}$ scheme, we vary the intermediate scale $\bar{\mu}$ between 3 GeV and 10 GeV and estimate the error from the unknown value of the conversion coefficient $\delta m_3^{\overline{\text{MS}}}$ as described in Section 3.3. All scheme conversion errors are added in quadrature.
- Charm-mass effects. As detailed in Section 3.5 we take the difference between the mass values at NNLO with and without charm effects.
- Non-perturbative effects. To estimate the order of magnitude, we follow [6] (see also [59]) and consider the leading contribution to the operator product expansion (OPE) from the gluon condensate. It is assumed that higher-dimensional condensates and higher-order corrections to the Wilson coefficients can be neglected. Note that the OPE is only valid for $m_b v^2 \sim m_b/n \gg \Lambda_{\text{QCD}}$. The need to avoid an uncontrolled, non-perturbative ultrasoft contribution limits the admissible values of n . Under these assumptions we find a negligible effect of less than 1 MeV on the value of the bottom mass.

The smallness of the gluon condensate contribution to moments of order $n = 10$ is surprising, since the corresponding contribution to the $\Upsilon(1S)$ is large (though uncertain, see the recent discussion in [28]) and the high moments are already completely determined by the $\Upsilon(1S)$. While a certain amount of cancellation of non-perturbative effects is expected in the moments due to quark–hadron duality, the degree of cancellation (about one part in 500 for $n = 10$) is somewhat puzzling. We therefore advocate that the estimate of non-perturbative effects from the gluon condensate correction is considered with some caution and refrain from using it to limit the allowed values of n . More details on the gluon condensate contribution are given in Appendix E.

Our results for the $\overline{\text{MS}}$ masses obtained from moments \mathcal{M}_n with $6 \leq n \leq 15$ are shown in Fig. 4. There appears to be a good agreement of the mass values extracted from moments with $n \approx 10$ and a reasonable convergence of the perturbation series. For smaller values of n the behaviour is considerably worse as the non-relativistic approximation becomes less reliable. As can be seen from Fig. 5, the mass values at NNNLO decrease due to the small continuum cross section near threshold (cf. Section 4.2). The behaviour is worse if “expanded” moments \mathcal{M}_n are considered (lower panel).

As anticipated in Section 3.4 there is a considerable difference between the mass values extracted from “unexpanded” moments $\widetilde{\mathcal{M}}_n^{\text{th}}$ and “expanded” moments $\mathcal{M}_n^{\text{th}}$. For the tenth moment the mass difference amounts to -26 MeV. Though quite large, this value still lies within our error estimate for higher-order contributions obtained by varying the renormalisation scale.

As our final result we adopt the PS and $\overline{\text{MS}}$ masses extracted from the 10th moment $\widetilde{\mathcal{M}}_{10}^{\text{th}}$ leading to

$$\begin{aligned}
 m_b^{\text{PS}}(2 \text{ GeV}) &= [4.532_{-0.035}^{+0.002}(\mu) \pm 0.010(\alpha_s)_{-0}^{+0.003}(\text{res}) \pm 0.001(\text{conv}) \\
 &\quad \pm 0.002(\text{charm})_{-0.013}^{+0.007}(n) \pm 0.003(\text{exp})] \text{ GeV} \\
 &= 4.532_{-0.039}^{+0.013} \text{ GeV},
 \end{aligned} \tag{4.1}$$

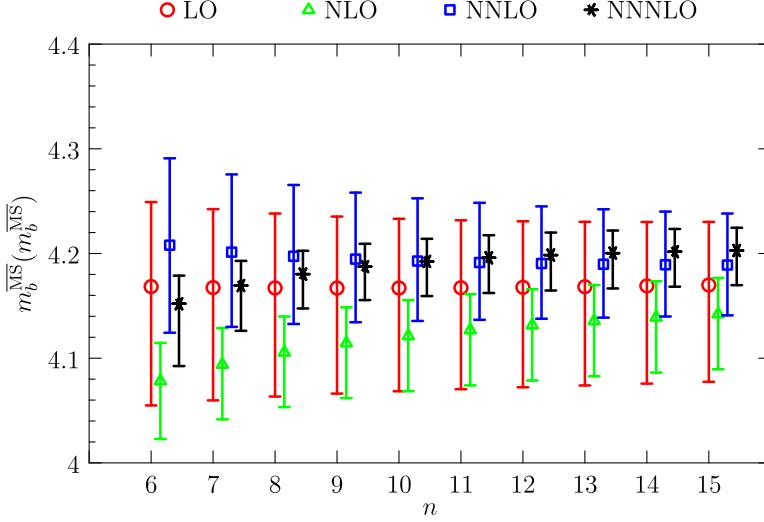


Fig. 4. Values of $m_b^{\overline{\text{MS}}}(m_b^{\overline{\text{MS}}})$ in GeV obtained from m_b^{PS} for different moments \mathcal{M}_n .

$$\begin{aligned}
 m_b^{\overline{\text{MS}}}(m_b^{\overline{\text{MS}}}) &= [4.193_{-0.031}^{+0.002}(\mu) \pm 0.001(\alpha_s)_{-0}^{+0.003}(\text{res})_{-0.010}^{+0.021}(\text{conv}) \\
 &\quad \pm 0.002(\text{charm})_{-0.012}^{+0.006}(n) \pm 0.003(\text{exp})] \text{ GeV} \\
 &= 4.193_{-0.035}^{+0.022} \text{ GeV.}
 \end{aligned} \tag{4.2}$$

In addition to the uncertainties discussed above we added the differences to the central mass values obtained from $\tilde{\mathcal{M}}_8^{\text{th}}$ and $\tilde{\mathcal{M}}_{12}^{\text{th}}$ to our error estimate. The corresponding term is marked by the label (n). Our value for the $\overline{\text{MS}}$ mass is in good agreement with determinations from relativistic (small n) sum rules at order α_s^3 [12] and approximate NNNLO non-relativistic sum-rules [11]. A more detailed comparison is given in Section 4.4.

An alternative method is to forego the PS scheme and directly use relation (3.11) to eliminate the pole mass in favour of the $\overline{\text{MS}}$ mass. For this “direct” extraction of the $\overline{\text{MS}}$ mass we obtain

$$\begin{aligned}
 m_b^{\overline{\text{MS}}}(m_b^{\overline{\text{MS}}}) &= [4.194_{-0.026}^{+0.001}(\mu) \pm 0.001(\alpha_s)_{-0}^{+0.003}(\text{res})_{-0.010}^{+0.008}(\text{conv}) \\
 &\quad \pm 0.002(\text{charm})_{-0.013}^{+0.007}(n) \pm 0.003(\text{exp})] \text{ GeV} \\
 &= 4.194_{-0.030}^{+0.012} \text{ GeV.}
 \end{aligned} \tag{4.3}$$

4.4. Comparison with previous works

As can be seen from Table 3, recent sum rule determinations of the bottom-quark mass are in reasonably good agreement.⁷ In the following we summarise the differences between the listed analyses.

⁷ We do not include NNNLO determinations of the bottom-quark mass from the $\Upsilon(1S)$ mass, since the theoretical uncertainty is dominated by non-perturbative effects (see e.g. [8]) and is not competitive with those given in Table 3.

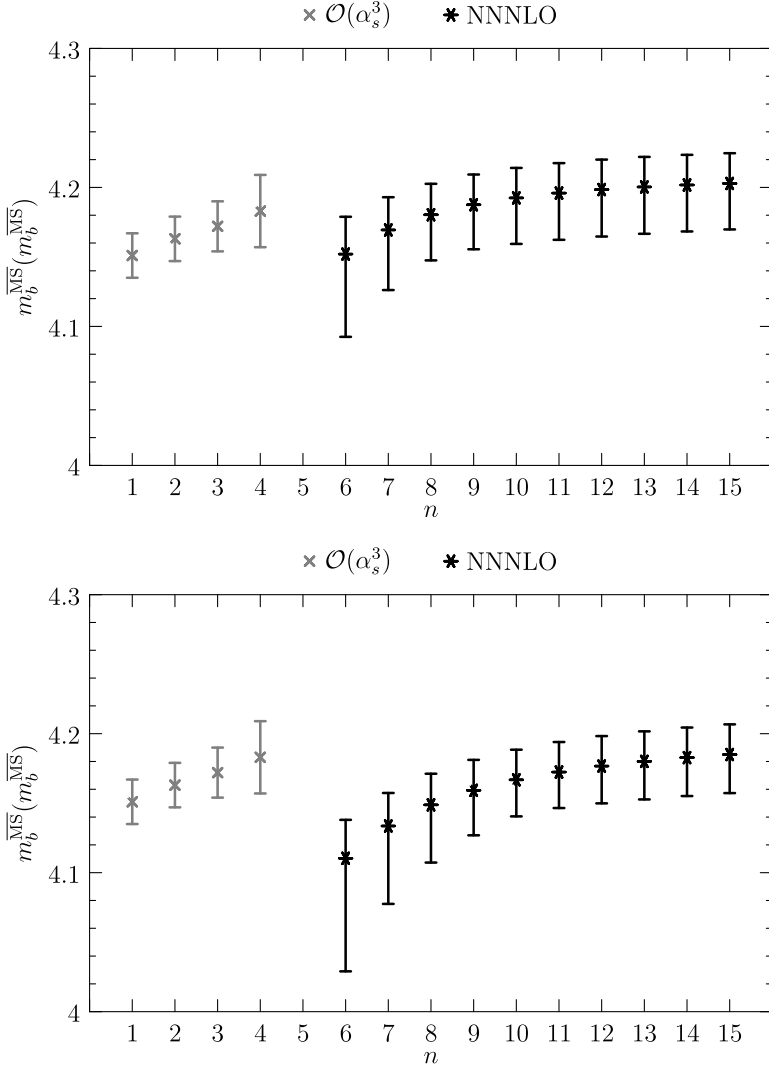


Fig. 5. Values of $m_b^{\overline{\text{MS}}}(m_b^{\overline{\text{MS}}})$ in GeV obtained from m_b^{PS} for different NNNLO moments \mathcal{M}_n with $6 \leq n \leq 15$. In the upper panel we show the resulting mass values for “unexpanded” theoretical moments defined according to (3.15); in the lower panel we have used “expanded” moments (3.5). To facilitate the comparison to existing results we include the mass values obtained from a fixed-order determination [12] for $n \leq 4$.

Table 3
Bottom-quark masses obtained from different sum rule analyses. In the last column experimental and theoretical errors were added in quadrature.

Analysis	Central moment	Perturbative order	$m_b^{\overline{\text{MS}}}(m_b^{\overline{\text{MS}}})$ [GeV]
CKMMSS [12]	\mathcal{M}_2	α_s^3	4.163 ± 0.016
HRS [13]	\mathcal{M}_{10}	NNLO + NNLL	4.235 ± 0.055
PZ [11]	\mathcal{M}_{15}	approx. NNNLO	4.169 ± 0.009
This work	\mathcal{M}_{10}	NNNLO	$4.193^{+0.022}_{-0.035}$

4.4.1. Chetyrkin et al. (CKMMSS) [12]

CKMMSS consider relativistic moments \mathcal{M}_n , $n \leq 4$, in fixed-order perturbation theory to order α_s^3 . Our experimental input largely corresponds to the one used by CKMMSS. However, as low moments are much more sensitive to the experimental high-energy continuum, CKMMSS rely on the prediction from perturbation theory above 11.24 GeV and use a linear interpolation between this region and the last data point at 11.2062 GeV. CKMMSS choose the same scale for the strong coupling and the $\overline{\text{MS}}$ mass and estimate the perturbative uncertainty from correlated scale variation and an estimated upper bound for the α_s^4 coefficient. Since we vary the two scales independently, the perturbative error estimates are not directly comparable. We expect however that an independent scale variation generally yields a more conservative error estimate. Conversely, if we set $\bar{\mu} \equiv \mu$ in our analysis we obtain $m_b^{\overline{\text{MS}}}(m_b^{\overline{\text{MS}}}) = 4.194_{-0.029}^{+0.012}$ GeV in place of (4.2) with a significantly smaller estimated uncertainty. The more conservative error estimate using uncorrelated coupling and mass renormalisation scale variations that should be compared to our result (4.2) or (4.3) is unfortunately not available.

4.4.2. Hoang, Ruiz-Femenía and Stahlhofen (HRS) [13]

HRS perform a renormalisation group improved analysis of the moments \mathcal{M}_n with $6 \leq n \leq 14$ and a default value of $n = 10$ in the framework of vNRQCD [60]. In addition to the usual terms scaling as $\alpha_s \sqrt{n}$ also logarithms $\alpha_s \ln \sqrt{n}$ are summed, achieving NNLO + (partial) NNLL accuracy. Like CKMMSS, HRS use the perturbative QCD prediction in place of experimental data for the high-energy continuum, but assign an uncertainty of 10% to it. We agree with the experimental moments used by HRS within the errors. HRS first determine the so-called 1S mass, which is then converted to the $\overline{\text{MS}}$ scheme. The analysis of HRS does not include charm-mass effects, which are currently unknown in their renormalisation group improved framework.

HRS assume an uncertainty of 15 MeV in the conversion to the $\overline{\text{MS}}$ mass. This is comparable to our estimate, albeit slightly lower. Like HRS we find that the dependence on α_s is reduced by the conversion from the intermediate mass scheme to the $\overline{\text{MS}}$ scheme and is quite small in the final result.

The central values of our analysis at NNLO and NNNLO almost coincide, but lie about 45 MeV below the NNLL and about 80 MeV below the NNLO result obtained in HRS. The analysis of HRS differs from ours in a number of aspects. HRS use the 1S instead of the PS mass, expand the factor $1/s^{n+1}$ non-relativistically and expand the bound-state poles, the 1S-pole mass relation and the factor $1/s$ in the vacuum polarisation function. They choose the moment-dependent central scale $\mu = m_b(1/\sqrt{n} + 0.2)$ instead of $\mu = m_b$, but use the hard scale for the vector current matching coefficients. Furthermore, HRS neglect charm-mass effects and use the $\overline{\text{MS}}$ -pole mass relation at order α_s^3 . We find that it is mainly the scale choice which is responsible for the difference between the NNLO results given by HRS and ours. The remaining differences in the analyses have only moderate numerical effects, though their precise size depends on the order in which they are implemented. As a net result, when we adapt our analysis to the one of HRS, we reproduce their NNLO value up to a negligible difference of 2 MeV. We note that the estimate of the perturbative uncertainty at NNLO based on the scale variation of HRS is about twice as large as the one used by us. Given that the convergence of the successive approximations from NNLO to NNNLO at the scale $\mu = m_b$ is very good (see Fig. 1), while low scales generally seem to lead to a break-down of non-relativistic perturbation theory [23], we conclude that our error estimate is sufficiently conservative.

The final result of HRS refers to the (partial) NNLL calculation. The resummation of logarithms reduces the scale dependence compared to the NNLO result and therefore compensates part of the large positive shift of the bottom-quark mass introduced by choosing a lower scale, leading to the bottom-quark mass quoted in Table 3. A previous less complete NNLO + partial NNLL analysis [61] obtained $m_b^{\overline{\text{MS}}}(m_b^{\overline{\text{MS}}}) = 4.19 \pm 0.06$.

4.4.3. Penin and Zerf (PZ) [111]

PZ also use non-relativistic sum rules, but choose even higher moments with a central value of $n = 15$. Such moments are rather insensitive to the experimental high-energy continuum, which in their work is neglected, but potentially introduce an unspecified systematic uncertainty from ultrasoft effects that may already be in the non-perturbative regime (further discussion in Appendix E). Choosing $n = 15$ instead of $n = 10$ increases the resulting mass value by approximately 12 MeV.

On the theory side, PZ employ the complete NNNLO PNRQCD prediction for the resonances, and an estimate of $R_b = \rho Z_1^{\text{NNNLO}} / Z_1^{\text{NNLO}} R^{\text{NNLO}}$, $0.5 \leq \rho \leq 2$, for the continuum to account for the (then) unknown NNNLO contribution. Our calculation shows that the true result lies somewhat below the band spanned by the variation of the auxiliary parameter ρ . Using rescaled NNLO instead of NNNLO for the continuum leads to an increase of about 5 MeV in the mass extracted from \mathcal{M}_{15} . Not expanding the factor $1/s$ in the polarisation function (cf. Section 3.4), however, again lowers the resulting mass value by about 17 MeV. PZ directly extract the $\overline{\text{MS}}$ mass without any intermediate threshold mass. As can be seen by comparing (4.3) and (4.2) the effect on the final value is relatively small. It should be noted that PZ estimate a large charm effect based on [49], amounting to a mass shift of about -25 MeV, while our calculation results in a shift of only about -3 MeV (see discussion in Section 3.5). Neglecting QED and charm effects in both analyses the central values for $m_b^{\overline{\text{MS}}}(m_b^{\overline{\text{MS}}})$ coincide (4.195 GeV vs. 4.194 GeV).

Notwithstanding the similarities between the two analyses, PZ claim a much smaller overall uncertainty of only 9 MeV in the value of the bottom-quark mass. The main reasons for this are overly optimistic estimates of the perturbative uncertainty and the uncertainty assigned to the conversion between pole and $\overline{\text{MS}}$ mass, where PZ assume 2.1 and 2.2 MeV, respectively, resulting in a significant overestimate of the final precision of the bottom-quark mass.

5. Conclusions

We have presented the first complete NNNLO determination of the bottom-quark mass from non-relativistic sum rules. We find a mass of $m_b^{\text{PS}}(2 \text{ GeV}) = 4.532_{-0.039}^{+0.013}$ in the PS scheme, which corresponds to an $\overline{\text{MS}}$ mass of $m_b^{\overline{\text{MS}}}(m_b^{\overline{\text{MS}}}) = 4.193_{-0.035}^{+0.022}$. Compared to previous NNLO analyses of non-relativistic moments we observe a significantly reduced uncertainty. This reduction is mostly due to the choice of a higher central scale $\mu = m_b^{\text{PS}}$, which follows from better insight into the convergence of successive approximations which are now known up to NNNLO. In spite of poor behaviour of the continuum cross section we observe that the NNNLO moments are stable under scale variation, and moments with different $n \approx 10$ are in good agreement with each other. Our results agree reasonably well with other recent determinations of the bottom-quark mass from the inclusive $e^+e^- \rightarrow b\bar{b}$ cross section, including NNNLO fixed-order analyses based on relativistic sum-rules. Conservative uncertainty estimates of the bottom-quark $\overline{\text{MS}}$ mass have now reached the $\pm(25\text{--}30)$ MeV range.

Acknowledgements

This work has been supported by the DFG Sonderforschungsbereich/Transregio 9 “Compu-tergestützte Theoretische Teilchenphysik”, the Gottfried Wilhelm Leibniz programme of the Deutsche Forschungsgemeinschaft (DFG), and the Munich Institute for Astro- and Particle Physics (MIAPP) of the DFG cluster of excellence “Origin and Structure of the Universe”. Some analytical calculations were performed with the help of FORM [62].

Appendix A. Charm effects in the Coulomb potential

To determine the effects of a non-zero charm-quark mass we split the Coulomb potential into two parts

$$\tilde{V} = \tilde{V}_{\text{massless}} + \tilde{V}_{m_c}, \quad (\text{A.1})$$

where $\tilde{V}_{\text{massless}}$ refers to the Coulomb potential for a massless charm quark, so that the charm correction \tilde{V}_{m_c} vanishes for $m_c = 0$.

The corrections to the Coulomb potential due to the charm-quark mass have been determined at NNLO in [50,51]. We use the following dispersion relation representations from [49], which are very convenient for computations. In momentum space the potential is given by

$$\tilde{V}_{m_c}(\mathbf{q}) = \sum_{i=1}^{\infty} \delta \tilde{V}_{m_c}^{(i)}(\mathbf{q}), \quad (\text{A.2})$$

$$\delta \tilde{V}_{m_c}^{(1)}(\mathbf{q}) = -\frac{4\pi\alpha_s C_F}{\mathbf{q}^2} \frac{\alpha_s}{3\pi} T_F \left[\Pi(\mathbf{q}^2) - \left(\ln \frac{\mathbf{q}^2}{m_c^2} - \frac{5}{3} \right) \right], \quad (\text{A.3})$$

$$\begin{aligned} \delta \tilde{V}_{m_c}^{(2)}(\mathbf{q}) = & -\frac{4\pi\alpha_s C_F}{\mathbf{q}^2} \left(\frac{\alpha_s}{4\pi} \right)^2 \left\{ \frac{8T_F}{3} \left[\Pi(\mathbf{q}^2) - \left(\ln \frac{\mathbf{q}^2}{m_c^2} - \frac{5}{3} \right) \right] \left(a_1 - \beta_0 \ln \frac{\mathbf{q}^2}{\mu^2} \right) \right. \\ & + \left(\frac{4T_F}{3} \right)^2 \left[\Pi(\mathbf{q}^2) - \left(\ln \frac{\mathbf{q}^2}{m_c^2} - \frac{5}{3} \right) \right]^2 \\ & \left. + \frac{76T_F}{3} \left[\mathcal{E}(\mathbf{q}^2) - \left(\ln \frac{\mathbf{q}^2}{m_c^2} - \frac{161}{114} - \frac{26}{19} \zeta_3 \right) \right] \right\}, \end{aligned} \quad (\text{A.4})$$

where

$$a_1 = \frac{31}{9} C_A - \frac{20}{9} T_F n_l, \quad (\text{A.5})$$

$$\beta_0 = \frac{11}{3} C_A - \frac{4}{3} T_F n_l, \quad (\text{A.6})$$

$$\Pi(\mathbf{q}^2) = 2\mathbf{q}^2 \int_1^{\infty} dx \frac{f(x)}{\mathbf{q}^2 + 4x^2 m_c^2}, \quad (\text{A.7})$$

$$\mathcal{E}(\mathbf{q}^2) = 2c_1 \mathbf{q}^2 \int_{c_2}^{\infty} \frac{dx}{x} \frac{1}{\mathbf{q}^2 + 4x^2 m_c^2} + 2d_1 \mathbf{q}^2 \int_{d_2}^{\infty} \frac{dx}{x} \frac{1}{\mathbf{q}^2 + 4x^2 m_c^2}, \quad (\text{A.8})$$

$$f(x) = \frac{\sqrt{x^2 - 1}}{x^2} \left(1 + \frac{1}{2x^2} \right). \quad (\text{A.9})$$

The parameters c_1, c_2, d_1, d_2 are adopted from [49] as

$$c_1 = \frac{\ln \frac{A}{d_2}}{\ln \frac{c_2^2}{d_2}}, \quad d_1 = \frac{\ln \frac{c_2^2}{A}}{\ln \frac{c_2^2}{d_2}}, \tag{A.10}$$

$$c_2 = 0.470, \quad d_2 = 1.120, \tag{A.11}$$

$$A = \exp\left(\frac{161}{228} + \frac{13}{19}\zeta_3 - \ln 2\right). \tag{A.12}$$

The potential in configuration space can be obtained by a Fourier transformation. We obtain

$$\delta V_{m_c}^{(1)}(r) = -\frac{C_F \alpha_s}{r} \frac{\alpha_s}{3\pi} \left[\int_1^\infty dx f(x) e^{-2m_c r x} + \left(\ln(\tilde{m}_c r) + \frac{5}{6} \right) \right], \tag{A.13}$$

$$\begin{aligned} \delta V_{m_c}^{(2)}(r) = & -\frac{C_F \alpha_s}{r} \left(\frac{\alpha_s}{3\pi} \right)^2 \left\{ \left[-\frac{3}{2} \int_1^\infty dx f(x) e^{-2x m_c r} \right. \right. \\ & \times \left(\beta_0 \left[\ln \frac{4x^2 m_c^2}{\mu^2} - \text{Ei}(2x m_c r) - e^{4x m_c r} \text{Ei}(-2x m_c r) \right] - a_1 \right) \\ & + 3 \left(\ln(\tilde{m}_c r) + \frac{5}{6} \right) \left(\beta_0 \ln(\tilde{\mu} r) + \frac{a_1}{2} \right) + \beta_0 \frac{\pi^2}{4} \left. \right] \\ & - \left[\int_1^\infty dx f(x) e^{-2x m_c r} \left(\frac{5}{3} + \frac{1}{x^2} + \frac{\sqrt{x^2 - 1}(1 + 2x^2)}{2x^3} \ln \left(\frac{x - \sqrt{x^2 - 1}}{x + \sqrt{x^2 - 1}} \right) \right) \right. \\ & + \int_1^\infty dx f(x) e^{-2x m_c r} \left(\ln(4x^2) - \text{Ei}(2x m_c r) - e^{4x m_c r} \text{Ei}(-2x m_c r) - \frac{5}{3} \right) \\ & - \left. \left(\ln(\tilde{m}_c r) + \frac{5}{6} \right)^2 - \frac{\pi^2}{12} \right] \\ & \left. + \frac{57}{4} \left[c_1 \Gamma(0, 2c_2 m_c r) + d_1 \Gamma(0, 2d_2 m_c r) + \ln(\tilde{m}_c r) + \frac{161}{228} + \frac{13}{19} \zeta_3 \right] \right\}, \tag{A.14} \end{aligned}$$

where

$$\tilde{m}_c = m_c e^{\gamma_E}, \quad \tilde{\mu} = \mu e^{\gamma_E}. \tag{A.15}$$

In (A.13) we have corrected some typos in Eq. (30) of [49]. This also affects an integral representation in [49] that should read

$$e^{-x} \text{Ei}(x) + e^x \text{Ei}(-x) = \mathcal{P} \int_0^\infty dt \frac{2t e^{-xt}}{1-t^2}. \tag{A.16}$$

However, to our understanding this does not affect other parts of [49].

Appendix B. Charm effects in the relation between PS and pole mass

The PS mass at a subtraction scale μ_f is defined by [41]

$$m_b = m_b^{\text{PS}}(\mu_f) - \frac{1}{2} \int_{|\mathbf{q}| < \mu_f} \frac{d^3 \mathbf{q}}{(2\pi)^3} \tilde{V}(|\mathbf{q}|) = m_b^{\text{PS}}(\mu_f) + \sum_{i=0}^{\infty} \delta m_i^{\text{PS}}. \quad (\text{B.1})$$

Defining the charm corrections to the PS–pole relation

$$\sum_{i=1}^{\infty} \delta m_{i,m_c}^{\text{PS}} = -\frac{1}{2} \int_{|\mathbf{q}| < \mu_f} \frac{d^3 \mathbf{q}}{(2\pi)^3} \tilde{V}_{m_c}(|\mathbf{q}|), \quad (\text{B.2})$$

we obtain

$$\delta m_{1,m_c}^{\text{PS}} = \frac{\alpha_s}{\pi} C_F \mu_f \frac{\alpha_s}{4\pi} \frac{4}{3} T_F \left(I_{\Pi}(z) + I_{\ln}(m_c) + \frac{5}{3} \right), \quad (\text{B.3})$$

$$\begin{aligned} \delta m_{2,m_c}^{\text{PS}} = & \frac{\alpha_s}{\pi} C_F \mu_f \left(\frac{\alpha_s}{4\pi} \right)^2 \frac{4}{3} T_F \left[\frac{4}{3} T_F \left(I_{\Pi^2}(z) + 2I_{\Pi,\ln}(z, m_c) + I_{\ln,\ln}(m_c, m_c) \right) \right. \\ & + \frac{10}{3} (I_{\Pi}(z) + I_{\ln}(m_c)) + \frac{25}{9} \\ & + 2\beta_0 \left(I_{\Pi,\ln}(z, \mu) + I_{\ln,\ln}(m_c, \mu) + \frac{5}{3} I_{\ln}(\mu) \right) \\ & + 19 \left(c_1 I_{\mathcal{E}} \left(\frac{z}{c_2^2} \right) + d_1 I_{\mathcal{E}} \left(\frac{z}{d_2^2} \right) + I_{\ln}(m_c) \right) \\ & \left. + 2a_1 \left(I_{\Pi}(z) + I_{\ln}(m_c) + \frac{5}{3} \right) + \frac{161}{6} + 26\zeta_3 \right] \end{aligned} \quad (\text{B.4})$$

with

$$z = \left(\frac{\mu_f}{2m_c} \right)^2, \quad (\text{B.5})$$

$$I_{\ln}(m) = \ln \frac{m^2}{\mu_f^2} + 2, \quad (\text{B.6})$$

$$I_{\ln,\ln}(m_0, m_1) = \ln \frac{m_0^2}{\mu_f^2} \ln \frac{m_1^2}{\mu_f^2} + 2 \ln \frac{m_0^2}{\mu_f^2} + 2 \ln \frac{m_1^2}{\mu_f^2} + 8, \quad (\text{B.7})$$

$$I_{\mathcal{E}}(\hat{z}) = 2 \frac{\arctan \sqrt{\hat{z}}}{\sqrt{\hat{z}}} + \ln(1 + \hat{z}) - 2, \quad (\text{B.8})$$

$$I_{\Pi}(z) = \frac{z}{5} \left[{}_2F_1 \left(\begin{matrix} 1 & 1 \\ 7/2 \end{matrix} \middle| -z \right) + \frac{1}{3} {}_3F_2 \left(\begin{matrix} 1 & 1 & 3/2 \\ 5/2 & 7/2 \end{matrix} \middle| -z \right) \right], \quad (\text{B.9})$$

$$\begin{aligned} I_{\Pi,\ln}(z, m) = & I_{\Pi}(z) \ln \frac{m^2}{\mu_f^2} + \frac{2}{15} z \left[{}_3F_2 \left(\begin{matrix} 1 & 1 & 3/2 \\ 5/2 & 7/2 \end{matrix} \middle| -z \right) \right. \\ & \left. + \frac{1}{3} {}_4F_3 \left(\begin{matrix} 1 & 1 & 3/2 & 3/2 \\ 5/2 & 5/2 & 7/2 \end{matrix} \middle| -z \right) \right], \end{aligned} \quad (\text{B.10})$$

$$\begin{aligned}
 I_{\Pi^2}(z) = & \frac{1}{45z^3} \left\{ z(-9 + z(48 + 785z)) \right. \\
 & - 6\sqrt{z(1+z)}(-3 + z(17 + 110z)) \operatorname{arsinh}(\sqrt{z}) \\
 & + 9(-1 + 5z + 20z^3) \operatorname{arsinh}(\sqrt{z})^2 \\
 & + z^{\frac{5}{2}}[-18\pi^2 + 36 \operatorname{arsinh}(\sqrt{z})(\ln(z) - 2\ln(-1 + \sqrt{1+z})) \\
 & \left. - 36 \operatorname{Li}_2((\sqrt{z} + \sqrt{1+z})^{-2}) + 144 \operatorname{Li}_2((\sqrt{z} + \sqrt{1+z})^{-1}) \right\}. \tag{B.11}
 \end{aligned}$$

The parameters c_1, c_2, d_1, d_2 are the same as in (A.10)–(A.12). $\operatorname{Li}_2(x) = \sum_{i=1}^{\infty} x^i/i^2$ denotes the dilogarithm and the ${}_pF_{p-1}$ are (generalised) hypergeometric functions. For the sake of brevity we refrain from rewriting the ${}_2F_1$ and ${}_3F_2$ functions in (B.9) and (B.10) in terms of elementary functions. $C_F = 4/3, C_A = 3, T_F = 1/2$ are the usual group factors and $n_l = 4$ is the number of light flavours, including the charm quark. α_s is defined with n_l active flavours, i.e. $\alpha_s = \alpha_s^{(n_l)}(\mu)$.

Eqs. (B.3)–(B.5) are parametrised in terms of the pole charm-quark mass. Employing the $\overline{\text{MS}}$ mass $m_c^{\overline{\text{MS}}}(\mu_c)$ instead, $\delta m_{2,m_c}^{\text{PS}}$ receives an additional contribution

$$\delta m_{2,m_c}^{\text{PS}} \rightarrow \delta m_{2,m_c}^{\text{PS}} + \frac{\alpha_s}{\pi} C_F \mu_f \left(\frac{\alpha_s}{4\pi} \right)^2 \frac{16}{3} T_F C_F \left(2 + 3 \ln \frac{\mu_c}{m_c^{\overline{\text{MS}}}(\mu_c)} \right) (1 - z I'_{\Pi}(z)) \tag{B.12}$$

with

$$I'_{\Pi}(z) = \frac{1}{2(z+1)} + \frac{z-2}{10(z+1)} {}_2F_1 \left(\begin{matrix} 1 & 1 \\ \frac{7}{2} \end{matrix} \middle| -z \right) - \frac{1}{30} {}_3F_2 \left(\begin{matrix} 1 & 1 & \frac{3}{2} \\ \frac{5}{2} & \frac{7}{2} \end{matrix} \middle| -z \right). \tag{B.13}$$

For our analysis we set μ_c to our overall renormalisation scale μ .

Appendix C. Charm corrections to bound-state energies and wave functions

Writing the bound-state energies and wave functions in the form

$$E_N = E_N^{(0)} \left(1 + \sum_{i=1}^{\infty} e_N^{(i)} \right), \tag{C.1}$$

$$|\psi_N(0)|^2 = |\psi_N^{(0)}(0)|^2 \left(1 + \sum_{i=1}^{\infty} f_N^{(i)} \right), \tag{C.2}$$

we can again split the higher-order terms $e_N^{(i)}, f_N^{(i)}$ into two parts

$$e_N^{(i)} = e_{N,\text{massless}}^{(i)} + e_{N,m_c}^{(i)}, \tag{C.3}$$

$$f_N^{(i)} = f_{N,\text{massless}}^{(i)} + f_{N,m_c}^{(i)}, \tag{C.4}$$

where $e_{N,\text{massless}}^{(i)}, f_{N,\text{massless}}^{(i)}$ are the respective corrections for the case of massless charm quarks. A general strategy for computing bound state corrections is described in detail in [25]. We refrain from repeating this discussion here. For $i = 1$ (NLO), the mass corrections originate from a single potential insertion into the Coulomb Green function. The $i = 2$ (NNLO) contributions can be split further into three parts

$$e_{N,m_c}^{(2)} = e_{N,\{m_c\}}^{(2)} + e_{N,\{m_c,m_c\}}^{(2)} + e_{N,\{m_c,\text{massless}\}}^{(2)}, \quad (\text{C.5})$$

$$f_{N,m_c}^{(2)} = f_{N,\{m_c\}}^{(2)} + f_{N,\{m_c,m_c\}}^{(2)} + f_{N,\{m_c,\text{massless}\}}^{(2)}, \quad (\text{C.6})$$

where the subscripts $\{m_c\}$ and $\{m_c, m_c\}$ denote single and double insertions of the potential V_{m_c} , respectively. $\{m_c, \text{massless}\}$ denotes the contribution from the mixed double insertion of one potential V_{m_c} and one potential V_{massless} . In the following we list our results for these corrections.

C.1. Single insertions

The corrections to the energy levels and wave functions from single insertions of V_{m_c} read

$$e_{N,m_c}^{(1)} = -2\Gamma(1/2)\Gamma(N)\frac{\alpha_s}{4\pi}\frac{1}{2\pi i}\int_{-i\infty}^{i\infty} du \xi_N^{-u} I^{(1)}(u) \sum_{i=1}^N \eta_c(u, i, N), \quad (\text{C.7})$$

$$e_{N,\{m_c\}}^{(2)} = \frac{4}{3}\Gamma(1/2)\Gamma(N)\left(\frac{\alpha_s}{4\pi}\right)^2\frac{1}{2\pi i}\int_{-i\infty}^{i\infty} du \xi_N^{-u} I^{(2)}(u) \sum_{i=1}^N \eta_c(u, i, N), \quad (\text{C.8})$$

$$f_{N,m_c}^{(1)} = -\Gamma(1/2)\Gamma(N+1)\frac{\alpha_s}{4\pi}\frac{1}{2\pi i}\int_{-i\infty}^{i\infty} du \xi_N^{-u} I^{(1)}(u) \sum_{i=1}^N \phi_c(u, i, N), \quad (\text{C.9})$$

$$f_{N,\{m_c\}}^{(2)} = \frac{2}{3}\Gamma(1/2)\Gamma(N+1)\left(\frac{\alpha_s}{4\pi}\right)^2\frac{1}{2\pi i}\int_{-i\infty}^{i\infty} du \xi_N^{-u} I^{(2)}(u) \sum_{i=1}^N \phi_c(u, i, N), \quad (\text{C.10})$$

where

$$\xi_N = \frac{\alpha_s C_F m_b}{2Nm_c}, \quad (\text{C.11})$$

$$\eta_c(u, i, N) = \frac{\Gamma(-u)\Gamma(u+2)}{\Gamma(N-i+1)\Gamma(i)^2\Gamma(i+1)} \frac{\Gamma(u+i)}{\Gamma(u-i+2)}, \quad (\text{C.12})$$

$$\phi_c(u, i, N) = \eta_c(u, i, N) \left(\frac{3-u}{N} - \psi(N+1) + 2\psi(i) + \psi(i+1) - \psi(u+i) - \psi(u-i+2) \right), \quad (\text{C.13})$$

$$I^{(1)}(u) = \frac{\Gamma(2-\frac{u}{2})}{u\Gamma(\frac{5-u}{2})}, \quad (\text{C.14})$$

$$\begin{aligned} I^{(2)}(u) = & \frac{2\Gamma(3-\frac{u}{2})}{(u-2)\Gamma(\frac{7-u}{2})} - \frac{\Gamma(2-\frac{u}{2})}{u\Gamma(\frac{5-u}{2})} \left(3a_1 - 3\beta_0 \ln\left(\frac{m_c^2}{\mu^2}\right) \right. \\ & \left. + (2+3\beta_0) \left[\frac{2}{u} + \psi\left(2-\frac{u}{2}\right) - \psi\left(\frac{5-u}{2}\right) - \ln(4) + \pi \cot\left(\frac{\pi}{2}u\right) \right] \right) \\ & + \left(-\frac{2}{3} \frac{\Gamma(\frac{u-5}{2})}{(u-6)\Gamma(\frac{u}{2}-2)} - 2 \frac{\Gamma(\frac{u-3}{2})}{(u-4)\Gamma(\frac{u}{2}-1)} + \frac{8}{3} \frac{\Gamma(\frac{u+1}{2})}{u\Gamma(\frac{u}{2}+1)} \right) \cot\left(\frac{\pi}{2}u\right) \\ & - \frac{38}{\sqrt{\pi}} \frac{1}{u} (c_1 c_2^u + d_1 d_2^u). \end{aligned} \quad (\text{C.15})$$

The integration contour is chosen such that $0 < \text{Re}(u) < 1$ on the real axis.⁸

Expressing the charm mass corrections in terms of the $\overline{\text{MS}}$ mass $m_c^{\overline{\text{MS}}}(\mu_c)$ changes the NNLO contributions as follows.

$$e_{N,\{m_c\}}^{(2)} \rightarrow e_{N,\{m_c\}}^{(2)} + \left(\frac{\alpha_s}{4\pi}\right)^2 \left[\frac{4}{3} + 2 \ln\left(\frac{\mu_c}{m_c^{\overline{\text{MS}}}(\mu_c)}\right) \right] \times \left(-8\Gamma(1/2)\Gamma(N) \frac{1}{2\pi i} \int_{-i\infty}^{i\infty} du u \xi_N^{-u} I^{(1)}(u) \sum_{i=1}^N \eta_c(u, i, N) \right), \quad (\text{C.16})$$

$$f_{N,\{m_c\}}^{(2)} \rightarrow f_{N,\{m_c\}}^{(2)} + \left(\frac{\alpha_s}{4\pi}\right)^2 \left[\frac{4}{3} + 2 \ln\left(\frac{\mu_c}{m_c^{\overline{\text{MS}}}(\mu_c)}\right) \right] \times \left(-4\Gamma(1/2)\Gamma(N+1) \frac{1}{2\pi i} \int_{-i\infty}^{i\infty} du u \xi_N^{-u} I^{(1)}(u) \sum_{i=1}^N \phi_c(u, i, N) \right). \quad (\text{C.17})$$

We checked that our results for the binding energy of the $\Upsilon(1S)$ resonance up to NNLO agree numerically with [49]. Furthermore, the energy levels $e_{N,m_c}^{(1)}$ as well as the wave function $f_{1,m_c}^{(1)}$ are in numerical agreement with [52].

C.2. Massive double insertion

For double insertions of the potential V_{m_c} we obtain the following corrections to the binding energies and the wave functions:

$$e_{N,\{m_c,m_c\}}^{(2)} = \left(\frac{\alpha_s}{4\pi}\right)^2 \frac{\pi}{\Gamma(N)^2} \left\{ \frac{h_{m_c}^{(0)}(N)}{N^2} [h_{m_c}^{(0)}(N)(7 + 4N\psi(N)) - 4h_{m_c}^{(1)}(N)] + 2 \sum_{\substack{s=1 \\ s \neq N}}^{\infty} \frac{h_{m_c}^{(0)}(s)^2}{s(s-N)} \right\} - e_{N,m_c}^{(1)} f_{N,m_c}^{(1)}, \quad (\text{C.18})$$

$$f_{N,\{m_c,m_c\}}^{(2)} = \left(\frac{\alpha_s}{4\pi}\right)^2 \frac{\pi}{\Gamma(N)^2} \left\{ \frac{1}{N^2} [h_{m_c}^{(1)}(N)^2 + h_{m_c}^{(0)}(N)(3h_{m_c}^{(0)}(N) - 4h_{m_c}^{(1)}(N)[1 + N\psi(N)] + h_{m_c}^{(2)}(N) + Nh_{m_c}^{(0)}(N)[4\psi(N) + N(2\zeta_2 + 2\psi(N)^2 - \psi^{(1)}(N))]] - \sum_{\substack{s=1 \\ s \neq N}}^{\infty} \frac{h_{m_c}^{(0)}(s)}{s(s-N)} \left[2h_{m_c}^{(1)}(s) - h_{m_c}^{(0)}(s) \left(2 + 2N\psi(N) + \frac{N}{N-s} \right) \right] \right\}. \quad (\text{C.19})$$

The coefficients $h_{m_c}^{(j)}$ for $j = 0, 1, 2$ are

⁸ The complete charm-quark contributions are actually obtained by choosing $-1 < \text{Re}(u) < 0$. The pole at $u = 0$ then corresponds to the contribution for massless charm quarks. Choosing a contour with $0 < \text{Re}(u) < 1$ thus amounts to subtracting this contribution, in agreement with our definitions (C.3), (C.4) of $e_{N,m_c}^{(i)}$ and $f_{N,m_c}^{(i)}$.

$$\begin{aligned}
h_{m_c}^{(j)}(s) &= \sum_{k=1}^s \frac{(-1)^k \Gamma(s+1)}{k \Gamma(k)^2 \Gamma(s-k+1)} \\
&\times \frac{1}{2\pi i} \int_{-i\infty}^{i\infty} du \xi_N^{-u} I^{(1)}(u) \frac{(k+u)\Gamma(k+u)^2 \Gamma(-u)}{\Gamma(1+k+u-N)} \kappa^{(j)}(u, 1+k+u-N),
\end{aligned} \tag{C.20}$$

with

$$\kappa^{(0)}(u, x) = 1, \tag{C.21}$$

$$\kappa^{(1)}(u, x) = u + N\psi(x), \tag{C.22}$$

$$\kappa^{(2)}(u, x) = u(u-1) + N\psi(x)(2u + N\psi(x)) - N^2\psi^{(1)}(x), \tag{C.23}$$

and ξ_N and $I^{(1)}(u)$ as defined in (C.11), (C.14). We again chose a contour with $0 < \text{Re}(u) < 1$. It should be noted that during numerical evaluation large cancellations arise between the summands in (C.20) so that typically high-precision arithmetic is required.

C.3. Mixed double insertion

Our result for the mixed double insertion of V_{m_c} and V_{massless} is

$$\begin{aligned}
e_{N, \{m_c, \text{massless}\}}^{(2)} &= \left(\frac{\alpha_s}{4\pi}\right)^2 \frac{4\sqrt{\pi}}{\Gamma(N)} (-1)^{N+1} \left\{ \frac{h_{\text{massless}}^{(0)}(N) h_{m_c}^{(0)}(N)}{N} \right. \\
&+ \frac{h_{\text{massless}}^{(-1)}(N)}{N^2} \left[h_{m_c}^{(1)}(N) - h_{m_c}^{(0)}(N) \left(\frac{7}{2} + N\psi(N) \right) \right] \\
&+ \left. \sum_{\substack{s=1 \\ s \neq N}}^{\infty} \frac{h_{\text{massless}}^{(-1)}(s) h_{m_c}^{(0)}(s)}{s(N-s)} \right\} - e_{N, m_c}^{(1)} f_{N, \text{massless}}^{(1)} - e_{N, \text{massless}}^{(1)} f_{N, m_c}^{(1)},
\end{aligned} \tag{C.24}$$

$$\begin{aligned}
f_{N, \{m_c, \text{massless}\}}^{(2)} &= \left(\frac{\alpha_s}{4\pi}\right)^2 \frac{2\sqrt{\pi}}{\Gamma(N)} (-1)^{N+1} \left\{ \frac{1}{2N^2} [2N(-N h_{\text{massless}}^{(1)}(N) h_{m_c}^{(0)}(N)) \right. \\
&+ h_{\text{massless}}^{(0)}(N) [-h_{m_c}^{(1)}(N) + h_{m_c}^{(0)}(N)(2 + N\psi(N))] \\
&- h_{\text{massless}}^{(-1)}(N) (h_{m_c}^{(2)}(N) - 2h_{m_c}^{(1)}(N)(2 + N\psi(N)) \\
&+ h_{m_c}^{(0)}(N) [6 + 4N\psi(N) + N^2(\psi(N)^2 - \psi^{(1)}(N) + 2\xi_2)]] \\
&+ \sum_{\substack{s=1 \\ s \neq N}}^{\infty} \frac{1}{s(N-s)} \left[-h_{\text{massless}}^{(-1)}(s) h_{m_c}^{(1)}(s) - N h_{\text{massless}}^{(0)}(s) h_{m_c}^{(0)}(s) \right. \\
&+ \left. h_{\text{massless}}^{(-1)}(s) h_{m_c}^{(0)}(s) \left(\frac{N}{N-s} + 2 + N\psi(N) \right) \right] \left. \right\},
\end{aligned} \tag{C.25}$$

where the coefficients $h_{m_c}^{(j)}$ are as defined in (C.20) and

$$h_{\text{massless}}^{(-1)}(s) \stackrel{s \leq N}{=} 2\beta_0 \frac{s}{N-s}, \quad (\text{C.26})$$

$$h_{\text{massless}}^{(-1)}(N) = -N[a_1 + 2\beta_0(L_N + S_1(N))], \quad (\text{C.27})$$

$$h_{\text{massless}}^{(-1)}(s) \stackrel{s > N}{=} 2\beta_0 \frac{N}{s-N}, \quad (\text{C.28})$$

$$h_{\text{massless}}^{(0)}(s) \stackrel{s \leq N}{=} \frac{1}{N-s} \left\{ -h_{\text{massless}}^{(-1)}(s) - a_1 s + 2\beta_0 [N(\psi(N-s) - \psi(N)) + s(S_1(N-s) - L_N)] \right\}, \quad (\text{C.29})$$

$$h_{\text{massless}}^{(0)}(N) = -2\beta_0(1 + S_1(N-1) + N\psi^{(1)}(N)), \quad (\text{C.30})$$

$$h_{\text{massless}}^{(0)}(s) \stackrel{s > N}{=} \frac{1}{s-N} \left\{ h_{\text{massless}}^{(-1)}(s) + a_1 s - 2\beta_0 [N(\psi(s-N) - \psi(N)) + s(S_1(s-N) - L_N) - 2] \right\}, \quad (\text{C.31})$$

$$h_{\text{massless}}^{(1)}(N) = \beta_0 \left[\frac{1}{N} + 2S_2(N-1) - N(\psi^{(2)}(N) + 4\zeta_3) \right]. \quad (\text{C.32})$$

Here $S_i(n) = \sum_{k=1}^n k^{-i}$ denote the generalised harmonic numbers of order i .

Appendix D. NLO charm effects in the non-relativistic current correlator

The perturbative expansion of $G(E)$ as defined in (3.3) can be written as

$$G(E) = G_0(E) + \sum_{i=1}^{\infty} \delta_i G(E). \quad (\text{D.1})$$

Splitting off contributions from a non-zero charm-quark mass we define

$$\delta_i G(E) = \delta_i G_{\text{massless}}(E) + \delta_i G_{m_c}(E) \quad (\text{D.2})$$

such that $\delta_i G_{m_c}(E)$ vanishes for $m_c \rightarrow 0$.

At NLO charm mass effects enter through single insertions of the potential (A.13). Following [25] we split the correction $\delta_1 G_{m_c}(E)$ into a part A with no additional Coulomb exchange between the quark and the anti-quark and a part B which resums all ladder diagrams with at least one Coulomb exchange. In contrast to the cases considered in [25] splitting the correction into two parts is not strictly necessary, but still helps to elucidate the structure of the result.

Part A corresponds to a two loop diagram, that will be computed in momentum space. This diagram has no ultraviolet divergence and can be calculated directly in $d = 3$ dimensions. We obtain

$$\begin{aligned} \delta_1 G_{m_c, A}(E) &= - \int \left[\prod_{i=1}^4 \frac{d^3 \mathbf{p}_i}{(2\pi)^3} \right] \tilde{G}_0^{(0\text{ex})}(\mathbf{p}_1, \mathbf{p}_2; E) \delta \tilde{V}_{m_c}^{(1)}(\mathbf{p}_3 - \mathbf{p}_2) \tilde{G}_0^{(0\text{ex})}(\mathbf{p}_3, \mathbf{p}_4; E) \\ &= \frac{m_b^2 \alpha_s C_F}{4\pi} \frac{\alpha_s}{4\pi} \frac{1}{2\pi i} \\ &\quad \times \int_{-i\infty}^{i\infty} du \frac{u(1-u)\Gamma(-u)^2 \Gamma(1/2-u)\Gamma(1/2+u)^2 \Gamma(u)^2}{4\pi(\xi/2)^{2u} \Gamma(1+2u)\Gamma(5/2-u)}, \end{aligned} \quad (\text{D.3})$$

where

$$\xi = \frac{\sqrt{-m_b E}}{m_c}, \quad (\text{D.4})$$

and the contour must be chosen such that $0 < \text{Re}(u) < 1/2$ on the real axis.

For part *B* we perform the calculation in position space. The result can be written as a two-dimensional Mellin-Barnes integral

$$\begin{aligned} \delta_1 G_{m_c, B}(E) &= - \int d^3 \mathbf{r} \delta V_{m_c}^{(1)}(\mathbf{r}) [G_0(0, \mathbf{r}; E)^2 - G_0^{(\text{0ex})}(0, \mathbf{r}; E)^2] \\ &= \frac{m_b^2 \alpha_s C_F}{4\pi} \frac{\alpha_s}{4\pi} \left(-\frac{\sqrt{\pi}}{\Gamma(-\lambda)} \right) \frac{1}{(2\pi i)^2} \\ &\quad \times \int_{-i\infty}^{i\infty} dw \Gamma(w+1-\lambda) \Gamma^*(-w-1) \Gamma(-w)^2 \\ &\quad \times \int_{-i\infty}^{i\infty} du I^{(1)}(u) \xi^{-u} \frac{\Gamma(2+u) \Gamma(-u) \Gamma(1+u+w)}{\Gamma(1+u-w)}, \end{aligned} \quad (\text{D.5})$$

with $I^{(1)}(u)$ as defined in (C.14) and

$$\lambda = \frac{\alpha_s C_F}{2\sqrt{-E/m_b}}. \quad (\text{D.6})$$

In the integral over the variable u the contour should be fixed such that $0 < \text{Re}(u) < 1$ on the real axis. Note that by choosing the contour to the right of the pole at $u = 0$ we have accounted for the subtraction term in the potential (A.13). The notation $\Gamma^*(-w-1)$ denotes that the contour should be chosen to the right of the first pole at $w = -1$. For positive E it can be fixed parallel to the imaginary axis with $-1 < \text{Re}(w) < 0$, since the real part of λ vanishes and left and right poles are separated. For positive integer values N of λ Eq. (D.5) contains poles in $N - \lambda$ due to the pinching of the contour in the complex w plane by left and right poles. These poles determine the charm mass corrections to the resonances as obtained in Appendix C.

Appendix E. Gluon condensate correction

The gluon condensate correction to the PNRQCD Green function is given by [59]

$$\begin{aligned} \delta_{\langle G^2 \rangle} G(E) &= -\frac{\langle 0 | \pi \alpha_s G^2 | 0 \rangle}{18} \int d^3 \mathbf{r} \int d^3 \mathbf{r}' (\mathbf{r} \cdot \mathbf{r}') G^{(0)}(0, \mathbf{r}; E) \\ &\quad \times G^{(8)}(\mathbf{r}, \mathbf{r}'; E) G^{(0)}(\mathbf{r}', 0; E), \end{aligned} \quad (\text{E.1})$$

where the superscript (0), (8) refers to the colour-singlet and colour-octet Coulomb Green function, respectively (cf. [17]). Proceeding as in [25], we find the representation

$$\delta_{\langle G^2 \rangle} G^{(0)}(E) = -\frac{\pi^2}{18} K \frac{m_b^2 \alpha_s C_F}{4\pi} \lambda^5 \sum_{s=0}^{\infty} \frac{s! H_{\langle G^2 \rangle}(s)^2}{(s+3)!(s+2+\lambda/8)}, \quad (\text{E.2})$$

where λ is defined in (D.6),

$$K = \frac{\langle \frac{\alpha_s}{\pi} G^2 \rangle}{m_b^4 (\alpha_s C_F)^6}, \quad (\text{E.3})$$

Table 4

The contribution of the $\Upsilon(1S)$ resonance and the remaining resonances together with the continuum (rest) to the moments is shown separately for the experimental, the perturbative, and the gluon condensate correction to the moments. The perturbative contributions are evaluated at NNNLO and the condensate corrections at LO with the input values $m_b^{\text{PS}}(2 \text{ GeV}) = \mu = 4.53 \text{ GeV}$, $\alpha_s = 0.220486$, $m_c = 0$, and $K = 0.012 \text{ GeV}^4 / (m_b^4(\alpha_s C_F)^6)$, where the pole mass m_b is computed from $m_b^{\text{PS}}(2 \text{ GeV})$ at LO according to (3.11).

n	8	10	12	16	20	24
$\mathcal{M}_n^{\text{exp}, \Upsilon(1S)} / \mathcal{M}_n^{\text{exp}}$	0.738	0.803	0.850	0.913	0.948	0.969
$\widetilde{\mathcal{M}}_n^{\text{pert}, \Upsilon(1S)} / \widetilde{\mathcal{M}}_n^{\text{pert}}$	0.769	0.814	0.849	0.899	0.932	0.953
$\widetilde{\mathcal{M}}_n^{\text{pert, rest}} / \widetilde{\mathcal{M}}_n^{\text{pert}}$	0.231	0.186	0.151	0.101	0.068	0.047
$\delta_{(G^2)} \widetilde{\mathcal{M}}_n^{\Upsilon(1S)} / \widetilde{\mathcal{M}}_n^{\text{pert}}$	1.711	1.842	1.953	2.135	2.281	2.404
$\delta_{(G^2)} \widetilde{\mathcal{M}}_n^{\text{rest}} / \widetilde{\mathcal{M}}_n^{\text{pert}}$	-1.713	-1.845	-1.957	-2.144	-2.296	-2.427
$\delta_{(G^2)} \widetilde{\mathcal{M}}_n / \widetilde{\mathcal{M}}_n^{\text{pert}}$	-0.002	-0.003	-0.005	-0.009	-0.015	-0.023

and

$$H_{(G^2)}(s) = -\frac{(s+3)!}{s!} \lambda \frac{\Gamma(5)\Gamma(s-\lambda)}{\Gamma(5+s-\lambda)}. \tag{E.4}$$

The sum in (E.2) can be evaluated in terms of polygamma functions. Expanding (E.2) around the bound-state poles at $\lambda = N$ determines the condensate correction to the S -wave energy levels E_N and wave functions at the origin, $|\psi_N(0)|^2$ [63,64].

Eq. (E.2) can be integrated in the complex energy plane to yield the condensate contribution to the moments. It is worth noting that splitting this contribution into a resonance and continuum contribution is ill-defined, since the two are separately divergent. For the resonances the divergence arises in the sum over N , since the condensate correction rises too rapidly with principal quantum number N . For the continuum, the integral over energy is too singular at $E = 0$. This reminds us that the moment calculation really refers to the calculation of high derivatives of $\Pi_b(q^2)$ at $q^2 = 0$, and assumes the validity of the operator product expansion (OPE) for this quantity, for which the split into resonances and continuum contributions is artificial.

It is well-defined to split the condensate contribution into the one from the $\Upsilon(1S)$ resonance and the rest. The result normalised to the NNNLO theoretical moments (without the condensate contribution) is given in Table 4 together with the corresponding split-up of the perturbative contribution to the moment, and the experimental moment.

We first note that the theoretically computed, perturbative $\Upsilon(1S)$ contribution to the moments is very close to the experimental one. Both are large, increasing from 80% for the 10th moment to more than 95% for $n = 24$. Next, we observe that the gluon condensate correction to the $\Upsilon(1S)$ contribution to the moment is extremely large. Taken at face value, it exceeds the perturbative moment by a factor of about two. While there is a large ambiguity in the absolute size of the gluon condensate contribution (mainly related to the choice of scale in α_s in the expression for K), as discussed in [28], the enormous cancellation between the contribution to the $\Upsilon(1S)$ resonance, $\delta_{(G^2)} \widetilde{\mathcal{M}}_n^{\Upsilon(1S)} / \widetilde{\mathcal{M}}_n^{\text{pert}}$, and the remainder, $\delta_{(G^2)} \widetilde{\mathcal{M}}_n^{\text{rest}} / \widetilde{\mathcal{M}}_n^{\text{pert}}$, is independent of this size. For $n = 8$ it is effective to one part in 1000, and it remains at the 1% level even for very high moments $n = 24$. As a consequence, the total gluon condensate correction (last row in Table 4) remains very small, around 2%, for $n = 24$ when the ultrasoft scale m_b/n is clearly in the non-perturbative regime.

We believe that the validity of quark-hadron duality must be questioned when the experimental and perturbative contribution of the rest is a few percent, while the condensate contribution

to the same quantity is more than 50 times larger. It appears that the gluon condensate contribution to the entire moment is anomalously small. Further insight into the convergence of the OPE for high moments could be obtained from an estimate of the dimension-6 condensate contributions, which is not available. From power-counting the breakdown of the OPE is expected when $n\Lambda_{\text{QCD}}/m_b \sim 1$, which occurs in the ballpark of $n \sim 16$. If instead the maximal value of n was determined by the value at which the gluon condensate contribution is as large as the perturbative moment, we would find very large values of n , which seem to be clearly outside the range, where quark–hadron duality can be expected to apply.

References

- [1] V. Novikov, L. Okun, M.A. Shifman, A. Vainshtein, M. Voloshin, V.I. Zakharov, Sum rules for charmonium and charmed mesons decay rates in quantum chromodynamics, *Phys. Rev. Lett.* 38 (1977) 626.
- [2] V. Novikov, L. Okun, M.A. Shifman, A. Vainshtein, M. Voloshin, M. Voloshin, Charmonium and gluons: basic experimental facts and theoretical introduction, *Phys. Rep.* 41 (1978) 1–133.
- [3] R. Boughezal, M. Czakon, T. Schutzmeier, Four-loop tadpoles: applications in QCD, *Nucl. Phys. B, Proc. Suppl.* 160 (2006) 160–164, arXiv:hep-ph/0607141.
- [4] A. Maier, P. Maierhöfer, P. Marquard, Higher moments of heavy quark correlators in the low energy limit at $\mathcal{O}(\alpha_s^2)$, *Nucl. Phys. B* 797 (2008) 218–242, arXiv:0711.2636.
- [5] M. Voloshin, Y. Zaitsev, Physics of Υ resonances: ten years later, *Sov. Phys. Usp.* 30 (1987) 553–574.
- [6] M. Voloshin, Precision determination of α_s and m_b from QCD sum rules for $b\bar{b}$, *Int. J. Mod. Phys. A* 10 (1995) 2865–2880, arXiv:hep-ph/9502224.
- [7] A. Pineda, J. Soto, Effective field theory for ultrasoft momenta in NRQCD and NRQED, *Nucl. Phys. B, Proc. Suppl.* 64 (1998) 428–432, arXiv:hep-ph/9707481.
- [8] M. Beneke, A. Signer, The bottom $\overline{\text{MS}}$ quark mass from sum rules at next-to-next-to-leading order, *Phys. Lett. B* 471 (1999) 233–243, arXiv:hep-ph/9906475.
- [9] K. Melnikov, A. Yelkhovsky, The b quark low scale running mass from Υ sum rules, *Phys. Rev. D* 59 (1999) 114009, arXiv:hep-ph/9805270.
- [10] A. Hoang, $1S$ and $\overline{\text{MS}}$ bottom quark masses from Υ sum rules, *Phys. Rev. D* 61 (2000) 034005, arXiv:hep-ph/9905550.
- [11] A.A. Penin, N. Zerf, Bottom quark mass from Υ sum rules to $\mathcal{O}(\alpha_s^3)$, *J. High Energy Phys.* 1404 (2014) 120, arXiv:1401.7035.
- [12] K. Chetyrkin, J. Kühn, A. Maier, P. Maierhöfer, P. Marquard, M. Steinhauser, C. Sturm, Charm and bottom quark masses: an update, *Phys. Rev. D* 80 (2009) 074010, arXiv:0907.2110.
- [13] A. Hoang, P. Ruiz-Femenía, M. Stahlhofen, Renormalization group improved bottom mass from Υ sum rules at NNLL order, *J. High Energy Phys.* 1210 (2012) 188, arXiv:1209.0450.
- [14] Particle Data Group Collaboration, J. Beringer, et al., Review of particle physics (RPP), *Phys. Rev. D* 86 (2012) 010001.
- [15] F. Jegerlehner, Electroweak effective couplings for future precision experiments, *Nuovo Cimento C* 034S1 (2011) 31–40, arXiv:1107.4683.
- [16] BaBar Collaboration, B. Aubert, et al., Measurement of the $e^+e^- \rightarrow b\bar{b}$ cross section between $\sqrt{s} = 10.54$ GeV and 11.20 GeV, *Phys. Rev. Lett.* 102 (2009) 012001, arXiv:0809.4120.
- [17] M. Beneke, Y. Kiyo, K. Schuller, Third-order correction to top-quark pair production near threshold I. Effective theory set-up and matching coefficients, arXiv:1312.4791.
- [18] M. Beneke, A. Signer, V.A. Smirnov, Top quark production near threshold and the top quark mass, *Phys. Lett. B* 454 (1999) 137–146, arXiv:hep-ph/9903260.
- [19] P. Marquard, J.H. Piclum, D. Seidel, M. Steinhauser, Three-loop matching of the vector current, *Phys. Rev. D* 89 (2014) 034027, arXiv:1401.3004.
- [20] M.E. Luke, M.J. Savage, Power counting in dimensionally regularized NRQCD, *Phys. Rev. D* 57 (1998) 413–423, arXiv:hep-ph/9707313.
- [21] B.A. Kniehl, A.A. Penin, V.A. Smirnov, M. Steinhauser, Potential NRQCD and heavy quarkonium spectrum at next-to-next-to-next-to-leading order, *Nucl. Phys. B* 635 (2002) 357–383, arXiv:hep-ph/0203166.
- [22] A. Penin, V.A. Smirnov, M. Steinhauser, Heavy quarkonium spectrum and production/annihilation rates to order $\beta_0^3\alpha_s^3$, *Nucl. Phys. B* 716 (2005) 303–318, arXiv:hep-ph/0501042.

- [23] M. Beneke, Y. Kiyo, K. Schuller, Third-order Coulomb corrections to the S -wave Green function, energy levels and wave functions at the origin, Nucl. Phys. B 714 (2005) 67–90, arXiv:hep-ph/0501289.
- [24] M. Beneke, Y. Kiyo, K. Schuller, Third-order non-Coulomb correction to the S -wave quarkonium wave functions at the origin, Phys. Lett. B 658 (2008) 222–229, arXiv:0705.4518.
- [25] M. Beneke, Y. Kiyo, K. Schuller, Third-order correction to top-quark pair production near threshold II. Potential contributions, in preparation.
- [26] S. Wüster, Heavy quark potential at order α_s^2/m^2 , Diploma Thesis, Aachen, 2003 [in German].
- [27] B.A. Kniehl, A.A. Penin, M. Steinhauser, V.A. Smirnov, Nonabelian $\alpha_s^3/(m_q r^2)$ heavy-quark–anti-quark potential, Phys. Rev. D 65 (2002) 091503, arXiv:hep-ph/0106135.
- [28] M. Beneke, Y. Kiyo, P. Marquard, A. Penin, J. Piclum, D. Seidel, M. Steinhauser, Leptonic decay of the Upsilon(1S) meson at third order in QCD, Phys. Rev. Lett. 112 (2014) 151801, arXiv:1401.3005.
- [29] C. Anzai, Y. Kiyo, Y. Sumino, Static QCD potential at three-loop order, Phys. Rev. Lett. 104 (2010) 112003, arXiv:0911.4335.
- [30] A.V. Smirnov, V.A. Smirnov, M. Steinhauser, Three-loop static potential, Phys. Rev. Lett. 104 (2010) 112002, arXiv:0911.4742.
- [31] B.A. Kniehl, A.A. Penin, Ultrasoft effects in heavy quarkonium physics, Nucl. Phys. B 563 (1999) 200–210, arXiv:hep-ph/9907489.
- [32] M. Beneke, Y. Kiyo, A. Penin, Ultrasoft contribution to quarkonium production and annihilation, Phys. Lett. B 653 (2007) 53–59, arXiv:0706.2733.
- [33] M. Beneke, Y. Kiyo, Ultrasoft contribution to heavy-quark pair production near threshold, Phys. Lett. B 668 (2008) 143–147, arXiv:0804.4004.
- [34] M. Beneke, P. Falgari, S. Klein, C. Schwinn, Hadronic top-quark pair production with NNLL threshold resummation, Nucl. Phys. B 855 (2012) 695–741, arXiv:1109.1536.
- [35] J. Blümlein, Structural relations of harmonic sums and Mellin transforms up to weight $w = 5$, Comput. Phys. Commun. 180 (2009) 2218–2249, arXiv:0901.3106.
- [36] S. Albino, Analytic continuation of harmonic sums, Phys. Lett. B 674 (2009) 41–48, arXiv:0902.2148.
- [37] M. Beneke, V.M. Braun, Heavy quark effective theory beyond perturbation theory: renormalons, the pole mass and the residual mass term, Nucl. Phys. B 426 (1994) 301–343, arXiv:hep-ph/9402364.
- [38] I.I. Bigi, M.A. Shifman, N. Uraltsev, A. Vainshtein, The pole mass of the heavy quark. Perturbation theory and beyond, Phys. Rev. D 50 (1994) 2234–2246, arXiv:hep-ph/9402360.
- [39] M. Beneke, More on ambiguities in the pole mass, Phys. Lett. B 344 (1995) 341–347, arXiv:hep-ph/9408380.
- [40] I.I. Bigi, M.A. Shifman, N. Uraltsev, A.I. Vainshtein, High power n of m_b in beauty widths and $n = 5 \rightarrow \infty$ limit, Phys. Rev. D 56 (1997) 4017–4030, arXiv:hep-ph/9704245.
- [41] M. Beneke, A quark mass definition adequate for threshold problems, Phys. Lett. B 434 (1998) 115–125, arXiv:hep-ph/9804241.
- [42] A.H. Hoang, Z. Ligeti, A.V. Manohar, B decay and the Υ mass, Phys. Rev. Lett. 82 (1999) 277–280, arXiv:hep-ph/9809423.
- [43] A. Pineda, Determination of the bottom quark mass from the $\Upsilon(1S)$ system, J. High Energy Phys. 0106 (2001) 022, arXiv:hep-ph/0105008.
- [44] K. Chetyrkin, M. Steinhauser, The relation between the $\overline{\text{MS}}$ and the on-shell quark mass at order α_s^3 , Nucl. Phys. B 573 (2000) 617–651, arXiv:hep-ph/9911434.
- [45] K. Melnikov, T. van Ritbergen, The three-loop relation between the $\overline{\text{MS}}$ and the pole quark masses, Phys. Lett. B 482 (2000) 99–108, arXiv:hep-ph/9912391.
- [46] M. Beneke, V.M. Braun, Naive nonabelianization and resummation of fermion bubble chains, Phys. Lett. B 348 (1995) 513–520, arXiv:hep-ph/9411229.
- [47] P. Ball, M. Beneke, V.M. Braun, Resummation of $(\beta_0 \alpha_s)^n$ corrections in QCD: techniques and applications to the τ hadronic width and the heavy quark pole mass, Nucl. Phys. B 452 (1995) 563–625, arXiv:hep-ph/9502300.
- [48] C. Ayala, G. Cvetič, A. Pineda, The bottom quark mass from the $\Upsilon(1S)$ system at NNNLO, J. High Energy Phys. 1409 (2014) 045, arXiv:1407.2128.
- [49] A. Hoang, Bottom quark mass from Υ mesons: charm mass effects, arXiv:hep-ph/0008102.
- [50] M. Melles, Massive fermionic corrections to the heavy quark potential through two loops, Phys. Rev. D 58 (1998) 114004, arXiv:hep-ph/9805216.
- [51] M. Melles, The static QCD potential in coordinate space with quark masses through two loops, Phys. Rev. D 62 (2000) 074019, arXiv:hep-ph/0001295.
- [52] D. Eiras, J. Soto, Light fermion finite mass effects in non-relativistic bound states, Phys. Lett. B 491 (2000) 101–110, arXiv:hep-ph/0005066.

- [53] S. Bekavac, A. Grozin, D. Seidel, M. Steinhauser, Light quark mass effects in the on-shell renormalization constants, *J. High Energy Phys.* 0710 (2007) 006, arXiv:0708.1729.
- [54] K. Chetyrkin, J.H. Kühn, M. Steinhauser, RunDec: a Mathematica package for running and decoupling of the strong coupling and quark masses, *Comput. Phys. Commun.* 133 (2000) 43–65, arXiv:hep-ph/0004189.
- [55] A.G. Källén, A. Sabry, Fourth order vacuum polarization, *Kong. Dan. Vid. Sel. Mat. Fys. Med.* 29 (17) (1955) 1–20.
- [56] K. Chetyrkin, J.H. Kühn, M. Steinhauser, Three loop polarization function and $\mathcal{O}(\alpha_s^2)$ corrections to the production of heavy quarks, *Nucl. Phys. B* 482 (1996) 213–240, arXiv:hep-ph/9606230.
- [57] A.H. Hoang, V. Mateu, S. Mohammad Zebarjad, Heavy quark vacuum polarization function at $\mathcal{O}(\alpha_s^2)$ and $\mathcal{O}(\alpha_s^3)$, *Nucl. Phys. B* 813 (2009) 349–369, arXiv:0807.4173.
- [58] Y. Kiyo, A. Maier, P. Maierhöfer, P. Marquard, Reconstruction of heavy quark current correlators at $\mathcal{O}(\alpha_s^3)$, *Nucl. Phys. B* 823 (2009) 269–287, arXiv:0907.2120.
- [59] A.I. Onishchenko, B_c meson sum rules at next-to-leading order, arXiv:hep-ph/0005127.
- [60] M.E. Luke, A.V. Manohar, I.Z. Rothstein, Renormalization group scaling in nonrelativistic QCD, *Phys. Rev. D* 61 (2000) 074025, arXiv:hep-ph/9910209.
- [61] A. Pineda, A. Signer, Renormalization group improved sum rule analysis for the bottom quark mass, *Phys. Rev. D* 73 (2006) 111501, arXiv:hep-ph/0601185.
- [62] J. Vermaseren, New features of FORM, arXiv:math-ph/0010025.
- [63] M. Voloshin, Precoulombic asymptotics for energy levels of heavy quarkonium, *Sov. J. Nucl. Phys.* 36 (1982) 143.
- [64] H. Leutwyler, How to use heavy quarks to probe the QCD vacuum, *Phys. Lett. B* 98 (1981) 447.